

# Functional Evidence for the Involvement of Microtubules and Dynein Motor Complexes in TRIM5 $\alpha$ -Mediated Restriction of Retroviruses

Paulina Pawlica,<sup>a</sup> Valerie Le Sage,<sup>b</sup> Nolwenn Poccardi,<sup>a</sup> Michel J. Tremblay,<sup>c</sup> Andrew J. Mouland,<sup>b</sup> Lionel Berthoux<sup>a</sup>

Laboratory of Retrovirology, Department of Medical Biology and BioMed Group, Université du Québec à Trois-Rivières, Trois-Rivières, Québec, Canada<sup>a</sup>; HIV-1 RNA Trafficking Laboratory, Lady Davis Institute at the Jewish General Hospital and Department of Medicine, McGill University, Montréal, Québec, Canada<sup>b</sup>; Centre de Recherche en Infectiologie, Centre de Recherche du CHU de l'Université Laval, Québec, Canada<sup>c</sup>

## ABSTRACT

The tripartite motif (TRIM) family of proteins includes the TRIM5 $\alpha$  antiretroviral restriction factor. TRIM5 $\alpha$  from many Old World and some New World monkeys can restrict the human immunodeficiency virus type 1 (HIV-1), while human TRIM5 $\alpha$  restricts N-tropic murine leukemia virus (N-MLV). TRIM5 $\alpha$  forms highly dynamic cytoplasmic bodies (CBs) that associate with and translocate on microtubules. However, the functional involvement of microtubules or other cytoskeleton-associated factors in the viral restriction process had not been shown. Here, we demonstrate the dependency of TRIM5 $\alpha$ -mediated restriction on microtubule-mediated transport. Pharmacological disruption of the microtubule network using nocodazole or disabling it using paclitaxel (originally named taxol) decreased the restriction of N-MLV and HIV-1 by human or simian alleles of TRIM5 $\alpha$ , respectively. In addition, pharmacological inhibition of dynein motor complexes using erythro-9-(2-hydroxy-3-nonyl)adenine (EHNA) and small interfering RNA-mediated depletion of the dynein heavy chain (DHC) similarly decreased TRIM5 $\alpha$ -mediated restriction. The loss in restriction resulting from either the disassembly of microtubules or the disruption of dynein motor activity was seen for both endogenous and overexpressed TRIM5 $\alpha$  and was not due to differences in protein stability or cell viability. Both nocodazole treatment and DHC depletion interfered with the dynamics of TRIM5 $\alpha$  CBs, increasing their size and altering their intracellular localization. In addition, nocodazole, paclitaxel, and DHC depletion were all found to increase the stability of HIV-1 cores in infected cells, providing an alternative explanation for the decreased restriction. In conclusion, association with microtubules and the translocation activity of dynein motor complexes are required to achieve efficient restriction by TRIM5 $\alpha$ .

## IMPORTANCE

The primate innate cellular defenses against infection by retroviruses include a protein named TRIM5 $\alpha$ , belonging to the family of restriction factors. TRIM5 $\alpha$  is present in the cytoplasm, where it can intercept incoming retroviruses shortly after their entry. How TRIM5 $\alpha$  manages to be present at the appropriate subcytoplasmic location to interact with its target is unknown. We hypothesized that TRIM5 $\alpha$ , either as a soluble protein or a high-molecular-weight complex (the cytoplasmic body), is transported within the cytoplasm by a molecular motor called the dynein complex, which is known to interact with and move along microtubules. Our results show that destructuring microtubules or crippling their function decreased the capacity of human or simian TRIM5 $\alpha$  to restrict their retroviral targets. Inhibiting dynein motor activity, or reducing the expression of a key component of this complex, similarly affected TRIM5 $\alpha$ -mediated restriction. Thus, we have identified specific cytoskeleton structures involved in innate antiretroviral defenses.

Members of the tripartite motif (TRIM) family of proteins have been described to exhibit antiviral properties (1–4). The best-known member is TRIM5 $\alpha$ , first characterized as a factor from rhesus macaque (rhTRIM5 $\alpha$ ) that potently inhibits human immunodeficiency virus 1 (HIV-1) (5). Other TRIM5 $\alpha$  orthologs from some New World and Old World monkeys also provide protection against HIV-1 infection (6–8). Human TRIM5 $\alpha$  (huTRIM5 $\alpha$ ), while not having the ability to restrict HIV-1, protects against N-tropic murine leukemia virus (N-MLV) and equine infectious anemia virus (6, 7, 9–11). Expression of TRIM5 $\alpha$  is induced by type 1 interferons, supporting their role as innate immunity effectors (12, 13). In addition, TRIM5 $\alpha$  acts as an innate sensor of retroviral infections, triggering an antiviral signaling pathway that can lead to interferon production (14, 15).

Retroviral restriction is initiated by specific recognition of the N-terminal domain of incoming retroviral capsid (CA) proteins by the B30.2/PRYSPRY domain of TRIM5 $\alpha$  (16, 17). TRIM5 $\alpha$  binds to intact CA cores rather than monomeric CA proteins (18) and, as a result of this interaction, replication is impaired by sev-

eral effector mechanisms (reviewed in references 19, 20, and 21). Thus far, two major TRIM5 $\alpha$ -mediated blocks have been described. The first one is accelerated disassembly of the retroviral CA core accompanied by a decrease in amounts of reverse transcription products (17, 22–24). As a consequence of the disassembly induced by TRIM5 $\alpha$ , core components such as the viral RNA and integrase are solubilized or degraded (25). This restriction effector mechanism also involves the degradation of TRIM5 $\alpha$  by the proteasome in the presence of the restricted virus (26). Accordingly, treatment with proteasome inhibitors restores seem-

Received 16 December 2013 Accepted 1 March 2014

Published ahead of print 5 March 2014

Editor: W. I. Sundquist

Address correspondence to Lionel Berthoux, berthoux@uqtr.ca.

Copyright © 2014, American Society for Microbiology. All Rights Reserved.

doi:10.1128/JVI.03717-13

ingly normal disassembly of the viral core and rescues the production of viral cDNA (25, 27, 28). However, proteasome inhibition does not fully rescue infectivity in restrictive conditions, pointing to the existence of a second, proteasome-independent restriction mechanism. The precise mechanism of this second block is still unclear, but access of the viral DNA to the nucleus is inhibited (27, 29). This could be related to the “sequestration” of incoming retroviruses in cytoplasmic bodies (CBs) formed by TRIM5 $\alpha$  proteins (30, 31).

TRIM5 $\alpha$  contains a coiled-coil domain responsible for protein dimerization and a B-box domain important for the higher-order organized states that probably promote the formation of CBs (32, 33). CBs were described as dynamic structures constantly associating and disassociating with each other, exchanging TRIM5 $\alpha$  proteins with a pool of proteins diffused in the cytoplasm (34), and their size depends on the level of TRIM5 $\alpha$  expression (35). The role of CBs in retroviral restriction is still unclear, and some reports refute their relevance in this process (35, 36). Indeed, no CBs have been detected at endogenous TRIM5 $\alpha$  expression levels, and it is possible that some observed CBs are artifacts stemming from protein overexpression (36). On the other hand, TRIM5 $\alpha$  CBs were found to colocalize with ubiquitin (30), proteasomal subunits (31, 37), and p62/Sequestosome-1 (38). p62 is an important adaptor protein with a role in cell signaling and protein degradation (reviewed in references 39 and 40). In addition, TRIM5 $\alpha$  proteins form bodies that enclose incoming restriction-sensitive viruses and closely resemble preexisting CBs (30). Collectively, these observations suggest that TRIM5 $\alpha$  CBs are relevant to restriction mechanisms.

The microtubule network, a component of the cellular cytoskeleton, is made of highly dynamic filaments built of tubulin  $\alpha/\beta$  heterodimers and plays multiple roles in the cell, including intracellular transport, organelle positioning, and cell division (41). Microtubules provide platforms for molecular motors, which enable active transport through the dense cytoplasm of the cell. The dynein motor complex (reviewed in reference 42) is a microtubule-associated molecular motor that transports various cellular cargos toward the microtubule-organizing center (MTOC) at the minus-end of microtubules. The MTOC is found in the vicinity of the nucleus except during cell division. Several viruses, including HIV-1, were described as recruiting dynein motor complexes for their transport during the early stages of their replication (reviewed in references 43, 44, and 45). TRIM5 $\alpha$  CBs also associate with microtubules, and their movements along these filaments have been observed (34). However, a functional role for this association has not been demonstrated, nor have the molecular motors responsible for TRIM5 $\alpha$  movement been identified. We sought here to determine whether the integrity of microtubules was functionally important for restriction to occur. In addition, we investigated the role of the dynein motor in this process. Using pharmacological and genetic approaches coupled with imaging analyses, we provide evidence that both microtubules and dynein motor activity are important for the restriction process mediated by TRIM5 $\alpha$ .

## MATERIALS AND METHODS

**Cells, pharmaceuticals, and antibodies.** Human embryonic kidney 293T cells, human epithelial carcinoma HeLa cells, human U373-derived MAGI cells, rhesus macaque kidney FRhK-4 cells, and feline renal CRFK cells were maintained in Dulbecco modified Eagle medium (DMEM) with

high glucose, supplemented with 10% fetal bovine serum and antibiotics at 37°C and 5% CO<sub>2</sub>. All cell culture reagents were from HyClone (Thermo Scientific, Logan, UT). HeLa cells stably expressing FLAG-tagged TRIM5 proteins were generated by retroviral transduction as described previously (22, 46). Nocodazole, paclitaxel (originally named taxol), erythro-9-(2-hydroxy-3-nonyl)adenine (EHNA), 2,3-bis-(2-methoxy-4-nitro-5-sulphophenyl)-2H-tetrazolium-5-carboxanilide (XTT), phenazine methosulfate (PMS), heparin sodium salt, and cycloheximide were provided by Sigma (St. Louis, MO). Anti-dynein heavy chain (anti-DHC) rabbit polyclonal antibodies were obtained from Santa Cruz (Dallas, TX). The horseradish peroxidase (HRP)-conjugated mouse anti-actin antibody was from Sigma. Capsid (CA; p24) was detected by using a mouse monoclonal antibody (clone 183) from the AIDS Research and Reference Reagent Program. The FLAG epitope was detected using the M2 mouse monoclonal antibody (Sigma) or the M2 rabbit polyclonal antibody from Cell Signaling (Danvers, MA). HRP-conjugated goat anti-rabbit and goat anti-mouse antibodies used as secondary antibodies in Western blots were all from Santa Cruz.

**Plasmid DNAs and retroviral vectors production.** The plasmid encoding a green fluorescent protein (GFP)-tagged version of  $\alpha$ -tubulin (47) was a gift from Ali Saib. To produce viral vectors, 10-cm culture dishes of subconfluent HEK293T cells were cotransfected using polyethyleneimine (25 kDa; Polyscience) with the appropriate plasmids as follows. For wild-type (WT) or the G89V CA mutant of HIV-1<sub>CMV-GFP</sub>, we used 10  $\mu$ g of pTRIP<sub>CMV-GFP</sub>, 10  $\mu$ g of WT or G89V p $\Delta$ R8.9, and 5  $\mu$ g of pMD-G. For N-MLV<sub>GFP</sub> and B-MLV<sub>GFP</sub>, we used 10  $\mu$ g of pCNCG, 5  $\mu$ g of pMD-G and 10  $\mu$ g of pCIG3N (N-MLV<sub>GFP</sub>) or pCIG3B (B-MLV<sub>GFP</sub>). For HIV-1<sub>NL43-GFP</sub>, we used 10  $\mu$ g of pNL-GFP and 5  $\mu$ g of pMD-G. For SIV<sub>mac-GFP</sub>, we used 10  $\mu$ g of pSIV<sub>mac-GFP</sub> and 5  $\mu$ g of pMD-G (22, 46, 48–54). pNL4.3<sub>IRES-GFP</sub> (55) encodes a version of the HIV-1 NL4-3 strain (56) expressing GFP in addition to the viral proteins and was a gift from David N. Levy. Production of the corresponding virus (HIV-1<sub>NL43-IRES-GFP</sub>) was done by transfecting 10  $\mu$ g of the plasmid in subconfluent HEK293T cells in a 75-cm flask. Media were changed at 16 h posttransfection, and virus-containing supernatants were collected after an additional 32 h of culture. All viral stocks were clarified by centrifugation for 5 min at a relative centrifugal force (RCF) of 400. All viral vectors were titrated in permissive CRFK cell using GFP expression as a marker of successful transduction. In some experiments, reverse transcriptase activity was measured on virus stocks using the EnzCheck kit (Molecular Probes) according to the manufacturer's instructions.

**Viral challenges, pharmacological treatments, and RNA interference.** Cells were seeded in 24-well plates at 10<sup>5</sup> cells/well (HeLa, CRFK, and MAGI cells) or 5  $\times$  10<sup>4</sup> cells/well (FRhK-4 cells) and were challenged the next day with various retroviral vectors (HIV-1<sub>CMV-GFP</sub>, HIV-1<sub>G89V</sub>, HIV-1<sub>NL43-GFP</sub>, SIV<sub>mac-GFP</sub>, N-MLV<sub>GFP</sub>, or B-MLV<sub>GFP</sub>) or a replication-competent retrovirus (HIV-1<sub>NL43-IRES-GFP</sub>). When applicable, cells were pretreated for 15 min with nocodazole, paclitaxel, or EHNA, and infections were then performed in the presence of these drugs. Media were changed after 16 h, and at 48 h postinfection the cells were treated with trypsin and fixed in 2% formaldehyde (Fisher Scientific) in phosphate-buffered saline (PBS). The percentages of GFP-positive cells were then determined by analyzing 1  $\times$  10<sup>4</sup> to 3  $\times$  10<sup>4</sup> cells on a FC500 MPL cytometer (Beckman Coulter) using the CXP software. For the siRNA treatments, 2  $\times$  10<sup>5</sup> cells were plated in each 3.5-cm of a six-well plate and transfected with 40 nM small interfering RNA (siRNA) using Dharmafect 1 (Dharmacon). The siRNA against the heavy chain of dynein (DHC) has been previously described (57) and targets the sequence 5'-GATCAACATGACGGAATT. Control siRNA (purchased from Dharmacon) was designed to target a luciferase sequence (5'-CGTACGCGGAATTACTCGATT) absent in the human genome. At 48 h posttransfection, the cells were seeded in 24-well plates and were challenged the next day with retroviral vectors as described above.

**Stability assay.** A total of 10<sup>6</sup> HeLa cells stably expressing FLAG-rhTRIM5 $\alpha$  were seeded in six-well plates 1 day prior to the experiment.

For the siRNA treatments, cells were transfected 48 h before seeding, as described above. Cells were pretreated for 1 h with 100  $\mu$ g of cycloheximide/ml and then treated with the indicated drugs without removing cycloheximide and harvested at the indicated time points. Drug concentrations were as follows: nocodazole, 0.1  $\mu$ M; paclitaxel, 0.1  $\mu$ M; and EHNA, 600  $\mu$ M. Cells were lysed in cold stability buffer (100 mM Tris-HCl [pH 8.0], 100 mM NaCl, 0.5% NP-40) supplemented with Complete protease inhibitor cocktail (Roche, Bale, Switzerland) and processed for Western blotting. rhTRIM5 $\alpha$  was detected by using the anti-FLAG rabbit polyclonal antibody.

**Viability assay.** A total of  $1 \times 10^4$  HeLa cells or  $5 \times 10^3$  FRhK-4 cells were seeded per well in 96-well plates. The next day, the cells were washed with PBS, and the wells were replenished with 100  $\mu$ l of DMEM without phenol red supplemented with serum and serial dilutions of the tested drugs. After 16 h of incubation, 100  $\mu$ l of the PBS solution containing 50  $\mu$ g of XTT and 6  $\mu$ g of PMS was added. The cells were incubated 2 to 4 h at 37°C, and then the absorbance was read at 490 nm on a Synergy HT (Bio-Tek) plate reader and corrected for background values determined on blank samples.

**Fate-of-capsid assay.** To analyze postentry capsid disassembly, a protocol adapted from Perron et al. (9) was used as described earlier by Keckesova et al. (7). Briefly,  $3 \times 10^6$  HeLa cells seeded in 10-cm dishes were infected with HIV-1<sub>CMV-GFP</sub> at a multiplicity of infection (MOI) of  $\sim 2$ , as calculated on the permissive control cells. Then, 2 h later, virus-containing supernatants were removed, and the cells were rinsed once in PBS, followed by a gentle trypsinization treatment (a 1:1 trypsin-PBS mixture for 10 s at room temperature). Fresh medium containing the appropriate drugs was then added, and cells were incubated at 37°C at 5% CO<sub>2</sub> for an additional 4 h. The cells were then treated with trypsin and resuspended in ice-cold lysis buffer (100  $\mu$ M Tris-HCl [pH 8.0], 0.4 mM KCl, 2  $\mu$ M EDTA, Roche's Complete protease inhibitor) and disrupted with a Dounce homogenizer. Whole-cell lysate (WCL) samples were collected at this point. In order to remove cell debris and nuclei, lysates were centrifuged for 5 min at an RCF of 1,000 at 4°C and then layered on top of a 50% sucrose cushion prepared in STE buffer (100 mM NaCl, 10 mM Tris-HCl [pH 8.0], 1 mM EDTA). Particulate viral cores were sedimented by ultracentrifugation in a Sorval WX Ultra 100 ultracentrifuge at  $175,000 \times g$  for 2 h at 4°C. Pellets were resuspended in denaturing gel loading buffer and processed for CA Western blotting, together with whole-cell lysates. The postcentrifugation supernatants were collected from the fraction above the sucrose cushion, excluding the sucrose-supernatant interface.

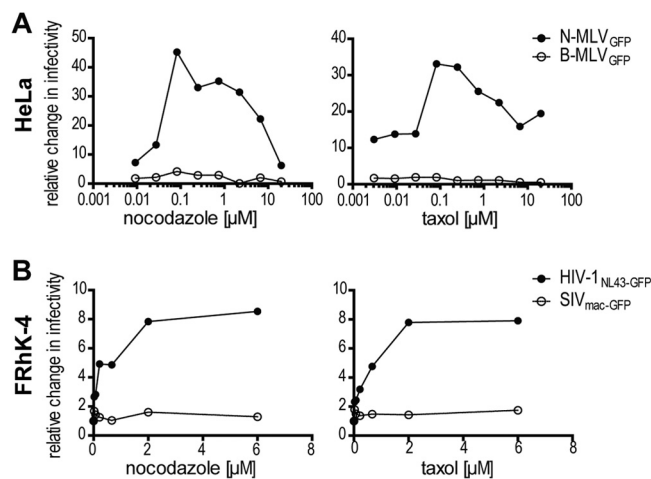
**Immunofluorescence (IF) microscopy.** For the analysis of the localization patterns of LAMP-1 and microtubules,  $2 \times 10^5$  cells (HeLa) or  $1 \times 10^5$  cells (FRhK-4) were seeded on glass coverslips placed in 3.5-cm wells. For siRNA treatments, cells were transfected 48 h prior to seeding as described above. For the cells expressing GFP-tubulin, 2  $\mu$ g of the plasmid were transfected per well 24 h prior to seeding. The day after seeding, cell were fixed (siRNA treatment) or incubated for 2 h with drugs (nocodazole, paclitaxel, and EHNA) and then fixed. Fixation was done for 10 min in prewarmed 4% formaldehyde-DMEM at 37°C, and then the cells were washed once in PBS, blocked in  $1 \times$  blocking solution (Roche), and stained or not for LAMP-1 for 1 h at room temperature. The primary rabbit LAMP-1 antibodies were described previously (57) and were diluted 1:1,000. LAMP-1 was revealed using the Alexa Fluor 594-conjugated donkey anti-rabbit secondary antibody (Molecular Probes, Eugene, OR). Cell nuclei were stained with DAPI (4',6'-diamidino-2-phenylindole; Invitrogen), washed with PBS, and mounted on glass slides using Immuno-Mount (Thermo-Fisher Scientific). Microscopy was performed using a microscope (DM16000B; Leica) equipped with a spinning disk confocal head (WaveFX; Quorum Technologies, Guelph, Ontario, Canada), a  $\times 63$  (1.4 numerical aperture oil immersion) plan Apochromat objective lens, and an electron microscopic charge-coupled device camera (ImageEM; Hamamatsu Photonics, Boston, MA). The Volocity Imaging software (v4.3.2; Perkin-Elmer, Waltham, MA) was used as acquisition software.

Image analyses were performed using the Imaris software v7.4 (Bitplane, Inc., South Windsor, CT). We estimated the effect of EHNA treatment or DHC depletion by determining the percentages of cells ( $n = 100$  to 300 in two experiments) exhibiting predominant LAMP-1 juxtanuclear staining versus cells exhibiting mostly peripheral staining, as described earlier (57).

For the analysis of TRIM5 $\alpha$  CBs and of microtubules, HeLa cells in 3.5-cm wells were transfected or not with siRNAs directed against DHC or Luciferase as described above. The next day, the cells were additionally transfected or not with 2  $\mu$ g of pGFP-tubulin per well using polyethyleneimine. The next day,  $2 \times 10^5$  of these cells were seeded on glass coverslips placed in 3.5-cm wells. After 24 h, the cells were treated or not with nocodazole for 4 h and then fixed and processed for IF staining. Fixation was done for 10 min in 4% formaldehyde-DMEM in 37°C, followed by three washes with ice-cold PBS. The cells were then permeabilized by treatment with 0.1% Triton X-100–0.1 mM sodium citrate for 1 to 2 min on ice. The cells were then washed again three times with PBS and treated with 10% normal goat serum (Sigma) containing 0.3 M glycine (Sigma) for 30 min at room temperature. This was followed by a 4-h incubation with a murine antibody against the FLAG epitope diluted 1:400 in PBS containing 10% normal goat serum. The cells were washed five times and fluorescently stained with the Alexa Fluor 594-conjugated goat anti-mouse antibody (Molecular Probes) at a 1:200 dilution. The cells were washed five times in PBS before mounting them in Vectashield (Vector Laboratories, Burlington, Ontario, Canada). Hoechst 33342 (0.8  $\mu$ g/ml; Molecular Probes) was added, along with the penultimate PBS wash, to visualize the DNA. Z-stacks were acquired on an AxioObserver microscope (Zeiss, Toronto, Ontario, Canada) equipped with the Apotome module, and median Z-stacks were retained for analysis. For the analysis of TRIM5 $\alpha$  CB sizes, FLAG foci in a given cell were manually outlined in the AxioVision software for calculation of the surface. A minimum of 100 and up to 214 CBs from 10 randomly chosen cells were included in the analysis. For the analysis of TRIM5 $\alpha$  CB localization, the cell's edge was outlined, and for each FLAG focus in a given cell, we measured the closest distance to the nuclear membrane and the closest distance to the plasma membrane using AxioVision. A minimum of 85 and up to 440 CBs from a minimum of five randomly chosen cells were included in the analysis. To avoid human bias, CBs size and localization analyses were performed blindly by students not otherwise involved in this project using image files that had coded names. For the analysis of TRIM5 $\alpha$  microtubule colocalization, images were acquired by using the Apotome in raw data mode to allow for subsequent deconvolution, which was done using the AxioVision software (Carl-Zeiss).

## RESULTS

**Nocodazole and paclitaxel treatments rescue the infectivity of retroviruses restricted by endogenous TRIM5 $\alpha$ .** In order to determine whether the microtubule network has a functional role in retroviral restrictions mediated by TRIM5 $\alpha$ , we used nocodazole and paclitaxel, pharmacological agents that prevent the polymerization of microtubules (58) or block their dynamics by preventing disassembly (59), respectively. First, we tested the effect of nocodazole and paclitaxel on the restriction of HIV-1 or N-MLV at multiple drug concentrations (Fig. 1). In this set of experiments, we infected human HeLa cells with N-MLV<sub>GFP</sub>, a huTRIM5 $\alpha$ -sensitive N-tropic MLV vector expressing GFP and, as a control, its restriction-insensitive B-tropic counterpart (B-MLV). Similarly, we infected rhesus macaque FRhK-4 cells with a rhTRIM5 $\alpha$ -sensitive HIV-1 vector expressing GFP or, as a control, with SIV<sub>mac-GFP</sub>, a rhTRIM5 $\alpha$ -insensitive simian immunodeficiency virus (SIV) strain mac239-based vector also expressing GFP. These infections were accomplished using virus doses that had been previously determined to result in 0.1 to 1% infected (GFP-positive) cells in the absence of drug. In these experimental conditions, we found that both nocodazole and paclitaxel in-



**FIG 1** Drug concentration-dependent enhancement of permissiveness to infection by TRIM5 $\alpha$ -restricted retroviral vectors in human and simian cells. HeLa cells (A) and FRhK-4 cells (B) were infected with single doses of the indicated viral vectors in the absence or presence of increasing amounts of nocodazole or paclitaxel (taxol) for 16 h. The amounts of viruses used were adjusted to obtain in the vicinity of 0.1 to 1% of infected cells in the absence of the drug and yielded 0.09% (N-MLV<sub>GFP</sub>), 0.38% (B-MLV<sub>GFP</sub>), 0.85% (HIV-1<sub>NL43-GFP</sub>), and 1.23% (SIV<sub>mac-GFP</sub>) infected cells. The percentages of infected (GFP-positive) cells were determined by flow cytometry at 2 days postinfection, and the results are presented as the fold changes in infectivity relative to the relevant untreated controls.

creased GFP transduction by the restricted virus while having little effect on infection by the unrestricted control virus (Fig. 1). Specifically, nocodazole treatment of cells increased N-MLV infection of HeLa cells by up to 45.2-fold and was active at a large range of concentrations peaking at  $\sim 0.1$   $\mu$ M (Fig. 1A). Nocodazole also increased the permissiveness of FRhK-4 cells to infection by HIV-1<sub>NL43-GFP</sub> by up to 8.5-fold (Fig. 1B). In these cells, nocodazole was active at higher concentrations ( $>0.5$   $\mu$ M). Nocodazole slightly increased infection by the unrestricted retroviral vector (B-MLV<sub>GFP</sub> or SIV<sub>mac-GFP</sub>) in both cell lines, but the magnitude of this effect reached  $\leq 4$ -fold and  $\leq 2$ -fold in HeLa and FRhK-4 cells, respectively (Fig. 1). This subtle enhancement in infection might be the result of cell cycle arrest mediated by nocodazole (60). Similar to nocodazole, paclitaxel increased N-MLV infection of HeLa cells by up to 33.1-fold (Fig. 1A). This enhancement was seen for all drug concentrations tested in HeLa cells, peaking at  $\sim 0.1$   $\mu$ M. increased HIV-1 infection of FRhK-4 cells by up to 7.9-fold (Fig. 1B) and, similar to nocodazole, higher concentrations of the drug ( $\geq 1$   $\mu$ M) needed to be used in this cell line in order to observe an effect on restriction. Paclitaxel slightly increased the infection of FRhK-4 cells by SIV<sub>mac-GFP</sub> (Fig. 1B) but, conversely, decreased B-MLV infectivity in HeLa cells at concentrations of  $>6$   $\mu$ M (Fig. 1A).

**Partial inhibition of TRIM5 $\alpha$ -mediated restriction by disruption of the microtubule network.** The experiments shown in Fig. 1 indicated that disruption of microtubules by nocodazole or paclitaxel treatments could increase infection by TRIM5 $\alpha$ -sensitive viruses but not TRIM5 $\alpha$ -insensitive ones. However, these results did not allow us to quantify the extent of inhibition conferred by nocodazole or paclitaxel treatments relative to the magnitude of the restriction itself. These results also did not allow us to analyze whether the effect seen was dependent on the MOI used.

Therefore, we performed virus dose-dependent experiments using fixed drug concentrations. We used nocodazole and paclitaxel concentrations that corresponded to their peak of antirestriction activity as determined in Fig. 1. When the virus amounts used were normalized according to the infectivity in nonrestrictive CRFK cells (CRFK infectious units [IU]), we found N-MLV<sub>GFP</sub> to be to  $\sim 500$ -fold less infectious than B-MLV<sub>GFP</sub> in HeLa cells (Fig. 2A), reflecting the expected level of N-MLV restriction by endogenous huTRIM5 $\alpha$  in these cells (7). Permissiveness to the huTRIM5 $\alpha$ -insensitive B-MLV vector was not significantly affected by either nocodazole or paclitaxel treatments, regardless of the virus amounts used (Fig. 2A). In contrast, N-MLV infectivity was increased by up to 65-fold after nocodazole treatment and by up to 71-fold after paclitaxel treatment (Fig. 2A). In other words, nocodazole and paclitaxel reduced restriction of N-MLV to a level of only  $\sim 20$ -fold in HeLa cells. In these cells, the effects of nocodazole and paclitaxel on N-MLV were greatest when a relatively small amount of virus was used (5 CRFK IU), whereas there was only an  $\sim 7$ -fold increase in N-MLV infection at MOIs 10-fold higher (Fig. 2A). These observations probably reflect the fact that saturation of endogenous huTRIM5 $\alpha$  by large amounts of N-MLV capsids partly suppresses restriction in the absence of pharmacological treatment.

As expected, HIV-1<sub>NL43-GFP</sub> was strongly restricted ( $\sim 1,000$ -fold) relative to SIV<sub>mac-GFP</sub> in macaque FRhK-4 cells, when the two viruses were normalized according to their infectious titers in CRFK cells (Fig. 2B) (49, 61). Nocodazole and paclitaxel had no effect on infection by SIV<sub>mac-GFP</sub>, regardless of the amount of virus used (Fig. 2B). In contrast, both nocodazole and paclitaxel increased infection by HIV-1<sub>NL43-GFP</sub> in these cells by 16- to 17-fold at low MOIs. When the virus dose used was  $>100$  CRFK IU, the enhancing effect of nocodazole and paclitaxel was smaller, which again was probably due to saturation of TRIM5 $\alpha$  by incoming capsids. The cyclophilin A (CypA) binding loop of CA is a major determinant of HIV-1 sensitivity to restriction by TRIM5 $\alpha$  (62), and the CA-G89V mutant, which abrogates CypA binding (63), is known to be less susceptible to restriction by rhTRIM5 $\alpha$  (49, 64). Thus, we hypothesized that nocodazole and paclitaxel treatments would have a smaller enhancing effect on CA-G89V HIV-1 compared to its WT counterpart. Indeed, we found that in subsaturating conditions ( $<200$  CRFK IU), nocodazole and paclitaxel increased WT HIV-1<sub>CMV-GFP</sub> by  $\sim 10$ -fold (5.6- to 16-fold) and  $\sim 7.5$ -fold (4.7- to 10.5-fold), respectively (Fig. 2C). In contrast, nocodazole and paclitaxel increased the infectivity of the mutant virus by only  $\sim 3.7$ -fold (2.3- to 5.0-fold) and  $\sim 3.4$ -fold (2.0- to 5.7-fold), respectively (Fig. 2C).

In order to verify that nocodazole and paclitaxel had the expected effect on the microtubule network in the cell lines used, we transfected a construct expressing a GFP- $\alpha$ -tubulin fusion in HeLa and FRhK-4 cells and then treated the cells with the same concentrations of nocodazole and paclitaxel as those used in Fig. 2A to C. The cells were then processed for IF analysis (Fig. 2D). Nocodazole prevents polymerization of microtubules (58) and, consequently, microtubules appeared shortened and/or disassembled; most of the signal was diffuse and distributed throughout the cytoplasm (Fig. 2D). Paclitaxel, on the other hand, binds to microtubule polymers to prevent their disassembly (59), resulting in the formation of abnormal microtubule bundles (65), a phenotype that was observed in both HeLa and FRhK-4 cell lines (Fig. 2D). Collectively, the data in Fig. 1 and 2 show that disrupting the

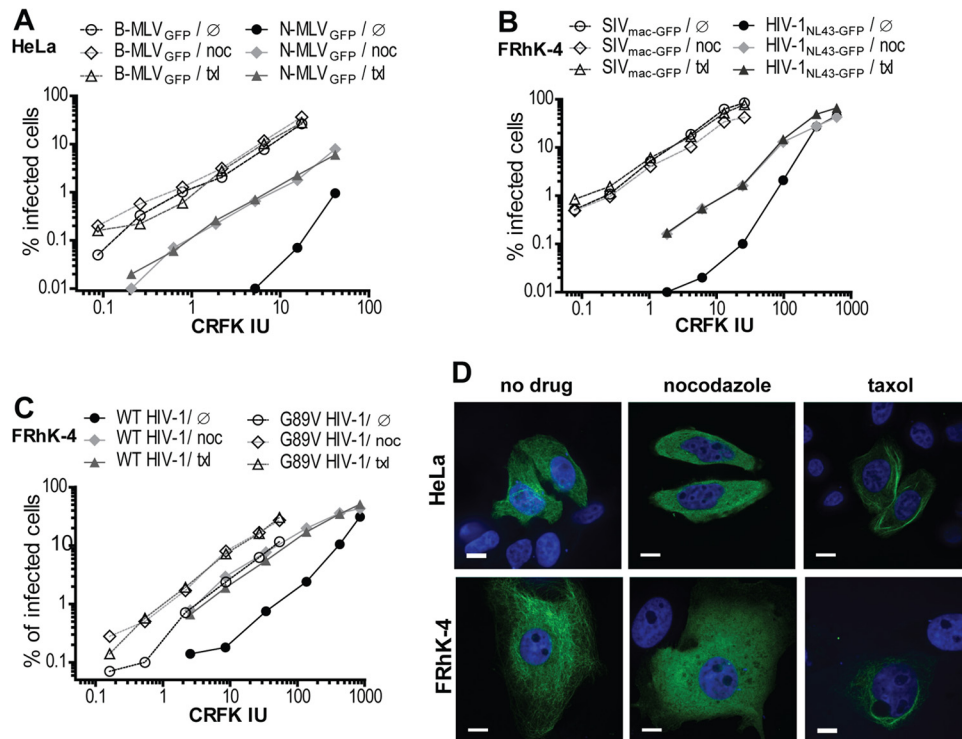


**FIG 2** Pharmacological disruption of microtubules decreases endogenous TRIM5 $\alpha$ -mediated retroviral restriction. (A to C) Effect of nocodazole (noc) and paclitaxel (txl) on restriction. Human HeLa cells (A) or macaque FRhK-4 cells (B and C) were infected with multiples doses of N-MLV<sub>GFP</sub>, B-MLV<sub>GFP</sub>, HIV-1<sub>NL43-GFP</sub>, or SIV<sub>mac-GFP</sub> as indicated. In panel C, FRhK-4 cells were infected with WT HIV-1<sub>CMV-GFP</sub> or with the CA-G89V mutant of this vector. Infections were performed for 16 h and in the absence of drug or in the presence of either nocodazole or paclitaxel. Nocodazole was used at 0.1  $\mu$ M in HeLa cells and at 6  $\mu$ M in FRhK-4 cells, and paclitaxel was used at 0.1  $\mu$ M in HeLa cells and at 2  $\mu$ M at FRhK-4 cells. The x axis in each graph represents the amounts of virus used expressed in infectious units (IU) based on infectious titers calculated for each virus in permissive feline CRFK cells. Infected (GFP-expressing) cells were detected by flow cytometry at 2 days postinfection. (D) IF microscopy analysis of microtubules in treated cells. HeLa and FRhK-4 cells were transfected with GFP- $\alpha$ -tubulin and 2 days later were subjected to 2-h drug treatments using the concentrations described above and then fixed. GFP fluorescence was observed by IF microscopy, along with DNA, which was stained using DAPI (blue staining). taxol, paclitaxel. The scale bars on the images represent 10  $\mu$ m. A representative image from each condition is presented.

dynamics (either assembly or disassembly) of microtubules results in a decrease of restriction by endogenous TRIM5 $\alpha$  without inhibiting it completely. Interestingly, when drug concentrations were optimized, we observed that nocodazole and paclitaxel had very similar effects on N-MLV or HIV-1 (Fig. 2A to C), suggesting that disruption of the microtubule network inhibited TRIM5 $\alpha$  regardless of the drug's mechanism of action.

**Pharmacological inhibition of dynein function rescues the infectivity of TRIM5 $\alpha$ -restricted retroviruses.** TRIM5 $\alpha$  CBs are associated with microtubules, and their movements within the cytoplasm seem to be at least partly dependent upon them (34). However, the molecular motors driving TRIM5 $\alpha$  CBs movements along microtubules are not known. We hypothesized that dynein played a role in TRIM5 $\alpha$  localization and contributed to its anti-retroviral activity. We first infected HeLa cells with N- or B-MLV<sub>GFP</sub> viral vectors in the presence of increasing concentrations of EHNA (Fig. 3A), a drug that inhibits the ATPase activity associated with the heavy chain of axonemal and cytoplasmic dyneins (66, 67). In the presence of EHNA, N-MLV<sub>GFP</sub> infectivity increased by up to 22-fold compared to the vehicle control, while the EHNA treatment caused a drug concentration-dependent decrease in permissiveness to B-MLV (Fig. 3A). In macaque FRhK-4 cells, EHNA increased permissiveness to HIV-1<sub>NL43-GFP</sub> by up to 18.5-fold in a drug concentration-dependent fashion (Fig. 3B). In

contrast, EHNA slightly decreased (<2-fold) infection by the restriction-insensitive SIV<sub>mac-GFP</sub>. We then performed the reverse experiments, infecting the cells at a fixed EHNA concentration but using multiple MOIs. Viruses were equalized as before, based on their titers in the nonrestrictive CRFK cells. In HeLa cells, treatment with 600  $\mu$ M EHNA had no effect on B-MLV<sub>GFP</sub> infectivity, but it increased permissiveness to N-MLV<sub>GFP</sub> infection by up to 22-fold, depending on the MOI (Fig. 3C). In FRhK-4 cells (Fig. 3D), EHNA (1.2 mM) enhanced HIV-1<sub>NL43-GFP</sub> infection at saturating MOIs ( $\leq 100$  CRFK IU) by 7.5-fold on average (3.2- to 13.5-fold). In contrast, EHNA caused a reduction in SIV<sub>mac-GFP</sub> infectivity to  $\sim 0.4$ -fold in the untreated control (Fig. 3D). Thus, the magnitude of HIV-1 enhancement by EHNA in FRhK-4 cells is probably underestimated in this experiment due to the negative effect of the drug on infectivity, as seen with SIV<sub>mac-GFP</sub>. In order to verify that the EHNA treatments indeed affected dynein function, we analyzed the subcellular distribution of LAMP-1, a marker for late endosomes (68). Impairment of dynein function causes a shift of late endosomes toward the cell periphery, as previously described by us (57) and others (69). Cells were stained for LAMP-1 after treatment or not with 600  $\mu$ M (HeLa) or 1.2 mM (FRhK-4) of EHNA. We then counted the number of cells exhibiting a juxtanuclear localization of LAMP-1 versus the ones with peripheral localization (Fig. 3E). In the dimethyl sulfoxide-treated

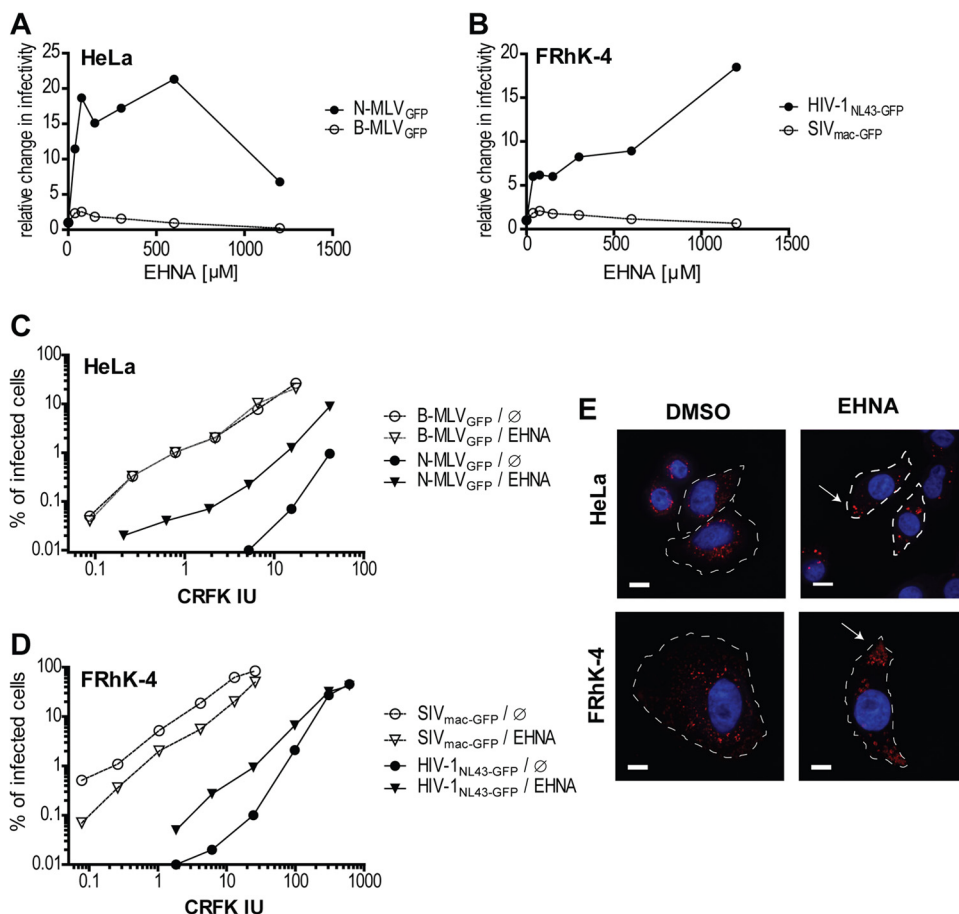


**FIG 3** Pharmacological disruption of dynein motor function decreases endogenous TRIM5 $\alpha$ -mediated retroviral restriction. (A and B) Dose-dependent effect of EHNA on restriction. Human HeLa cells (A) and macaque FRhK-4 cells (B) were infected for 16 h with a single dose of the indicated viruses in the presence of increasing concentrations of EHNA. The amounts of viruses used were the same as in Fig. 1. Infected (GFP-expressing) cells were detected by flow cytometry at 2 days postinfection. (C and D) Virus dose-dependent effect of EHNA on restriction. Human HeLa cells (C) and macaque FRhK-4 cells (D) were infected for 16 h with multiples doses of the indicated viruses in the presence or absence of EHNA at 600  $\mu$ M (HeLa) or 1.2 mM (FRhK-4). The x axis represents the amounts of virus used expressed in IU based on the infectious titers calculated for each virus in permissive feline CRFK cells. Infected (GFP-expressing) cells were detected by flow cytometry 2 days later. (E) IF microscopy analysis of LAMP-1 distribution. HeLa and FRhK-4 cells were treated for 2 h with EHNA or left untreated and then fixed and stained for the lysosomal marker LAMP-1 (red) and DNA (blue). Cell edges are outlined, and examples of localization shift caused by impaired dynein function are indicated by white arrows. A representative image from each condition is presented. The scale bars in the image panels represent 10  $\mu$ m.

control cells, the localization of LAMP-1 was predominantly juxtanuclear. Specifically, 92%  $\pm$  2.1% (the standard deviation) HeLa cells and 87%  $\pm$  1.5% FRhK-4 cells had juxtanuclear LAMP-1. As exemplified in Fig. 3E, EHNA treatment caused significant decreases in juxtanuclear LAMP-1, which represented 11%  $\pm$  4.6% and 8.6%  $\pm$  1.7% of total LAMP-1 in HeLa cells and FRhK-4 cells, respectively. In conclusion, EHNA can rescue both N-MLV and HIV-1 from restriction by different orthologs of endogenously expressed TRIM5 $\alpha$  but does not totally block restriction.

**Depletion of DHC counteracts TRIM5 $\alpha$ -mediated retroviral restriction.** In order to directly test the hypothesis that dynein function is important for TRIM5 $\alpha$ -mediated restriction, we depleted dynein heavy chain (DHC) by transfection of an siRNA, as described previously (57). Knocking down DHC is known to disrupt all dynein-mediated transport activities, and it can also affect the assembly of microtubules by inhibiting the anterograde transport of microtubule complexes (70). HeLa cells were transfected with a siRNA targeting DHC or with an irrelevant siRNA targeting

luciferase (Luc). Knockdown of DHC was efficient (Fig. 4A), resulting in an 85.4%  $\pm$  6.7% reduction in protein levels, as estimated by Western blotting in four independent experiments. In addition, DHC depletion caused a redistribution of LAMP-1 from juxtanuclear to peripheral (Fig. 4B), similar to what we had previously published (57). Specifically, 86.6% of HeLa cells transfected with the control siRNA had juxtanuclear staining compared to 35.5% for the cells transfected with the siRNA targeting DHC. As shown Fig. 4C, DHC knockdown caused a significant increase in HeLa permissiveness to N-MLV<sub>GFP</sub> infection at all MOIs examined (4.6-fold on average; range, 4.0- to 6.0-fold), while having no effect on infection by B-MLV<sub>GFP</sub>. Thus, dynein motor complexes are involved in the restriction of N-MLV by endogenous huTRIM5 $\alpha$ . Since dynein's transport function is dependent on microtubules, we predicted that combining pharmacological disruption of microtubules and DHC depletion would have nonadditive effects. Therefore, we analyzed the permissiveness to infection by N-MLV<sub>GFP</sub> and B-MLV<sub>GFP</sub> of cells depleted or not for DHC, in the presence of nocodazole or paclitaxel. As

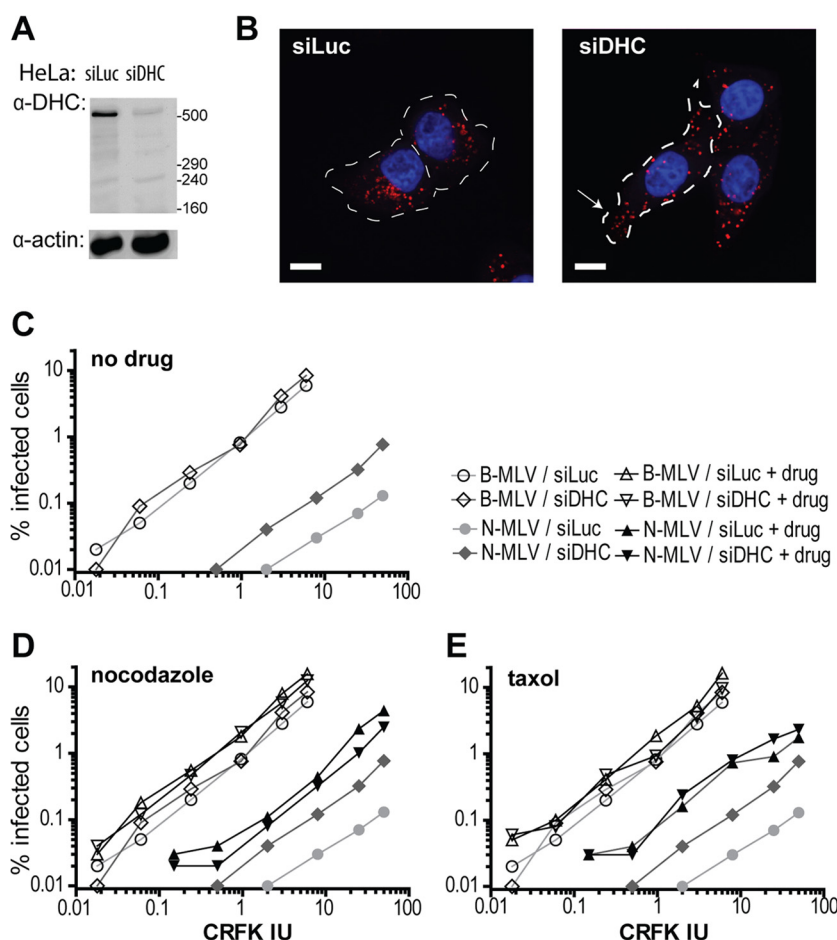


**FIG 4** DHC depletion decreases TRIM5 $\alpha$ -mediated retroviral restriction and has no effect on cells treated with nocodazole or paclitaxel. (A) Western blot analysis of DHC expression in HeLa cells 48 h after transfection of the indicated siRNAs. Actin was analyzed as a loading control. (B) IF microscopy analysis of LAMP-1. LAMP-1 was stained 72 h after siRNAs transfection (red), and DNA was stained using DAPI (blue). The cell edges are outlined, and a LAMP-1 distribution shift caused by impaired dynein function is indicated by a white arrow. A representative image is shown for each condition. The scale bars in the image panels represent 10  $\mu$ m. (C) Effect of DHC knockdown on restriction. Human HeLa cells were transfected with siRNAs against DHC (siDHC) or against luciferase (siLuc) as a control. After 72 h, the cells were infected for 16 h with multiple doses of N- or B-MLV<sub>GFP</sub>. Infected cells were detected by flow cytometry 2 days after infection. The x axis shows the amounts of virus used expressed in CRFK infectious units. (D and E) Effect of combining siRNA transfections with 0.25  $\mu$ M nocodazole (D) or 0.1  $\mu$ M paclitaxel (taxol) (E). Infections were performed and analyzed as in panel C, and panels C to E all share the symbol key.

shown in Fig. 4D, nocodazole alone increased N-MLV infection by an average of 23-fold (range, 11- to 34-fold), while dual treatment with nocodazole and DHC siRNAs resulted in a slightly smaller increase in N-MLV<sub>GFP</sub> infectivity (13-fold on average; range, 8- to 19-fold). Treatment with paclitaxel resulted in an average increase of 16.7-fold (range, 13- to 24-fold) in permissiveness to N-MLV<sub>GFP</sub>, and the enhancement effect was only slightly bigger (23-fold; range, 18- to 28-fold) when DHC depletion was combined with paclitaxel treatment (Fig. 4E). Altogether, the results in Fig. 4D and E show that disruption of the microtubule network and DHC depletion had non-additive effects on the restriction of N-MLV by endogenous huTRIM5 $\alpha$ . None of the treatments or combinations of treatments had a significant effect on the infectivity of the non-restricted B-MLV<sub>GFP</sub> control (Fig. 4C to E).

**Inhibition of HIV-1 restriction by overexpressed rhTRIM5 $\alpha$  in human cells is counteracted by depletion of DHC or microtubule disruption.** The experimental results shown in Fig. 1 to 4 indicate that restriction of HIV-1 or N-MLV by endogenous

huTRIM5 $\alpha$  or rhTRIM5 $\alpha$  cells is partly suppressed by DHC knockdown or by pharmacological disruption of microtubules using nocodazole or paclitaxel. We therefore decided to determine whether these interventions would also inhibit HIV-1 restriction in cells in which exogenous FLAG-tagged rhTRIM5 $\alpha$  was overexpressed. rhTRIM5 $\alpha$  was expressed in HeLa cells through retroviral transfer, and nontransduced cells were eliminated by puromycin treatment. We infected the transduced cells with the restriction-sensitive HIV-1 vectors HIV-1<sub>CMV-GFP</sub> and HIV-1<sub>NL43-GFP</sub>, as well as the rhTRIM5 $\alpha$ -insensitive SIV<sub>mac-GFP</sub> (Fig. 5A). The two vectors used differ in that HIV-1<sub>CMV-GFP</sub> does not carry the viral products Vpr, Nef, Vif, and Vpu, and no viral proteins are expressed following integration (71). In contrast, HIV-1<sub>NL43-GFP</sub> encodes all HIV-1 proteins with the exception of Env and Nef, and viral proteins are expressed in infected cells (72). Restriction was observed for both viruses in HeLa-rhTRIM5 $\alpha$  cells, compared to SIV<sub>mac-GFP</sub> and after normalization of viral stocks according to their titers on CRFK cells (Fig. 5A). Specifically, HIV-1<sub>CMV-GFP</sub> and HIV-1<sub>NL43-GFP</sub> were restricted ~40-fold and between ~48-

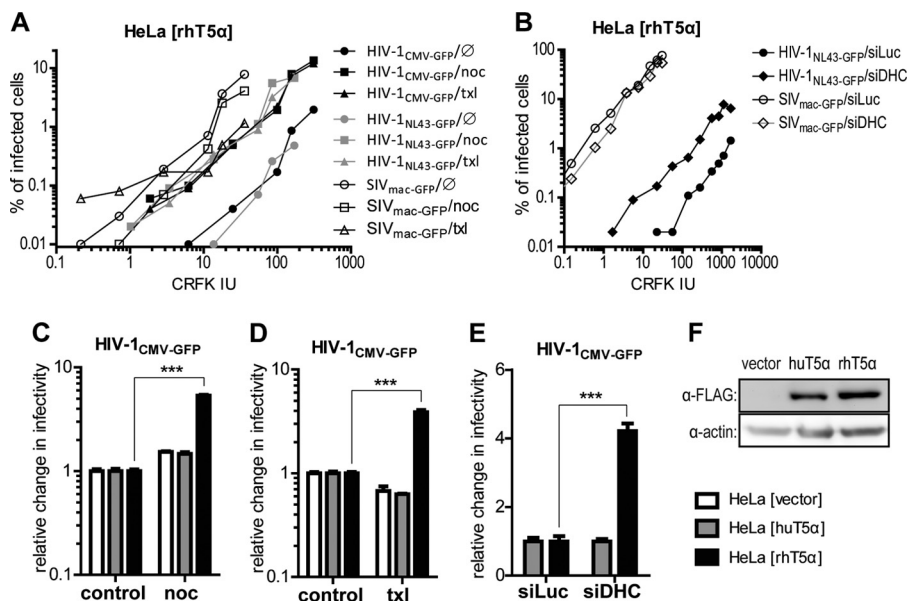


**FIG 5** Inhibition of HIV-1 restriction by rhTRIM5α exogenously expressed in HeLa cells. (A) Effect of nocodazole (noc) and paclitaxel (txl) on the restriction of HIV-1 vectors at multiple virus doses. HeLa cells stably expressing FLAG-tagged rhTRIM5α (rhT5α) were infected for 16 h with multiple amounts of the indicated vectors in the presence or absence of 0.1 μM nocodazole or paclitaxel. Virus doses were normalized according to titers in CRFK cells. The percentages of infected cells were analyzed at 2 days postinfection. (B) Effect of DHC depletion on the restriction of HIV-1<sub>NL43-GFP</sub>. HeLa cells stably expressing rhTRIM5α (rhT5α) were transfected with siRNAs targeting DHC (siDHC) or, as a control, luciferase (siLuc). The efficiency of DHC knockdown was similar to that in Fig. 4A (not shown). Cells were then infected for 16 h with HIV-1<sub>NL43-GFP</sub> or SIV<sub>mac-GFP</sub>, and the percentages of infected cells were determined 2 days later. (C and D) Effect of nocodazole or paclitaxel treatment on the infectivity of HIV-1<sub>CMV-GFP</sub> in cells expressing HIV-1 restrictive or nonrestrictive TRIM5α alleles. HeLa cells transduced as indicated with FLAG-tagged huTRIM5α (huT5α), FLAG-tagged rhTRIM5α (rhT5α), or empty vector were treated or not with 0.1 μM nocodazole (C) or 0.1 μM paclitaxel (D). Cells were simultaneously infected in triplicates with single doses of HIV-1<sub>CMV-GFP</sub> adjusted to yield ~1 to 10% of infected cells in the absence of the drug. Infectivities obtained in the absence of drugs are indicated in the figure as follows: (C) HeLa [vector], 1.23% ± 0.09%; HeLa [huT5α], 2.14 ± 0.81%; and HeLa [rhT5α], 0.82% ± 0.06%; and (D) HeLa [vector], 6.84% ± 0.14%; HeLa [huT5α], 6.58% ± 0.27%; and HeLa [rhT5α], 2.79% ± 0.19%. Infected cells were detected by flow cytometry at 2 days postinfection, and the results are presented as the fold changes relative to the relevant untreated controls (relative change in infectivity). (E) Effect of DHC depletion on restriction. HeLa cells stably expressing huTRIM5α or rhTRIM5α were transfected with siRNAs against DHC (siDHC) or against luciferase (siLuc) as a control and infected 72 h later in triplicates with single doses of the viral vector HIV-1<sub>CMV-GFP</sub> for 16 h. Virus doses were adjusted to obtain ~1% of infected cells for the siLuc control and yielded 1.61% ± 0.29% infected HeLa [huT5α] cells and 0.30% ± 0.08% infected HeLa [rhT5α] cells. Infected cells were detected by flow cytometry 2 days postinfection and results are presented as the fold changes relative to the relevant untreated controls (relative change in infectivity). \*\*\*,  $P < 0.0001$  (Student *t* test). (F) Western blotting of cells stably transduced with FLAG-tagged huTRIM5α and rhTRIM5α, with actin as a loading control.

and 78-fold, respectively. Nocodazole and paclitaxel increased permissiveness to HIV-1<sub>CMV-GFP</sub> by 10.1-fold and 9.8-fold, on average, and they increased permissiveness to HIV-1<sub>NL43-GFP</sub> by averages of 17.8- and 15.6-fold, respectively (Fig. 5A). None of the drug treatments had a significant effect on infection by SIV<sub>mac-GFP</sub>, although paclitaxel seemed to increase HIV-1 infectivity at relatively low MOIs and decrease it at relatively high MOIs (Fig. 5A). Next, we used FLAG-rhTRIM5α-transduced HeLa cells transfected with the control (luciferase-targeting) siRNA or with the siRNA targeting DHC (Fig. 5B). In this experiment, restriction of HIV-1<sub>NL43-GFP</sub> by rhTRIM5α was particularly high (>1,000-fold). We found that cells depleted of DHC were more permissive to infection by HIV-1<sub>NL43-GFP</sub> than cells transfected with the control siRNA (an 11.1-fold increase on average). In contrast, DHC knockdown slightly decreased infection by the control SIV<sub>mac-GFP</sub> vector (Fig. 5B).

In the next set of experiments (Fig. 5C to F), we compared the effect of nocodazole, paclitaxel, and DHC depletion on the permissiveness to HIV-1 of cells transduced with FLAG-rhTRIM5α or with a nonrestrictive control (huTRIM5α). The expression levels of huTRIM5α and rhTRIM5α were found to be comparable (Fig. 5F). Cells were infected at an MOI leading to ca. 1% infected

cells in the absence of treatment, as in Fig. 1. The addition of nocodazole increased the permissiveness of HeLa-rhTRIM5α cells to HIV-1<sub>CMV-GFP</sub> by (5.3 ± 0.21)-fold (Fig. 5C), while it had a much smaller effect on HeLa cells transduced with the “empty” vector (1.5 ± 0.04)-fold or HeLa cells transduced with huTRIM5α (1.46 ± 0.10)-fold. Likewise, treating the cells with paclitaxel increased permissiveness to HIV-1<sub>CMV-GFP</sub> by (3.9 ± 0.33)-fold (Fig. 5D), while it slightly decreased infection of HeLa vector and HeLa-huTRIM5α cells [(0.67 ± 0.13)-fold and (0.63 ± 0.12)-fold, respectively]. Depleting DHC similarly increased permissiveness to HIV-1<sub>CMV-GFP</sub> in cells expressing rhTRIM5α by (4.2 ± 0.38)-fold while having no effect in cells expressing the human ortholog (Fig. 5E). In conclusion, microtubule disruption with nocodazole and paclitaxel treatment and DHC depletion specifically inhibited the restriction of HIV-1 by exogenously expressed rhTRIM5α in human cells.

**Nocodazole and paclitaxel inhibit TRIM5α-mediated restriction of an HIV-1 vector bearing autologous envelope proteins.** The experiments shown in Fig. 1 to 5 were all performed using vesicular stomatitis virus protein G (VSV G)-pseudotyped vectors. TRIM5α-mediated restriction is not known to be affected by the mode of virus entry; nonetheless, we decided to verify that

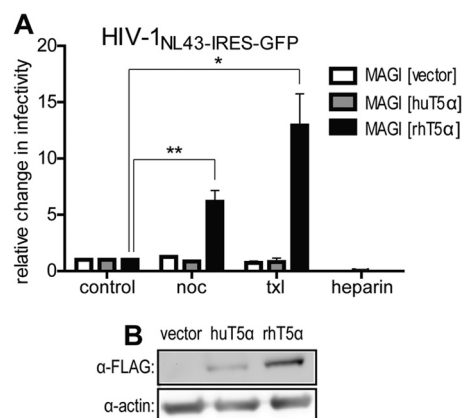


**FIG 6** Nodocazole and paclitaxel inhibit TRIM5 $\alpha$ -mediated restriction of nonpseudotyped HIV-1. (A) MAGI cells transduced with FLAG-tagged huTRIM5 $\alpha$  (huT5 $\alpha$ ), FLAG-tagged rhTRIM5 $\alpha$  (rhT5 $\alpha$ ), or the empty vector were treated or not with 0.25  $\mu$ M nodocazole (noc) or 0.1  $\mu$ M paclitaxel (txl). As a control, cells were also infected in the presence of the fusion inhibitor heparin (20  $\mu$ g/ml). Cells were infected in triplicates with single doses of HIV-1<sub>NL43-IRES-GFP</sub>. The amounts of virus used were adjusted to obtain  $\sim$ 0.1% of infected cells in the absence of the drug and yielded  $0.22\% \pm 0.025\%$  infected MAGI [vector] cells,  $0.16\% \pm 0.03\%$  infected MAGI [huT5 $\alpha$ ] cells, and  $0.043\% \pm 0.006\%$  infected MAGI [rhT5 $\alpha$ ] cells. Supernatants were replaced with fresh medium containing heparin at 16 h postinfection in order to prevent reinfections. Infected (GFP-positive) cells were detected by flow cytometry 2 days postinfection, and the results are presented as the fold changes in the percentages of infected cells relative to the relevant untreated controls (relative change in infectivity). \* and \*\*,  $P = 0.0134$  and  $P = 0.0068$ , respectively (Student  $t$  test). (B) Western blot analysis of FLAG-huTRIM5 $\alpha$  and FLAG-rhTRIM5 $\alpha$  expression in stably transduced MAGI cells. Actin was analyzed as a loading control.

nodocazole and paclitaxel would inhibit the TRIM5 $\alpha$ -mediated restriction of a virus bearing its autologous envelope. For that, we used a fully infectious HIV-1 clone (HIV-1<sub>NL43-IRES-GFP</sub>) encoding GFP in addition to all of the other viral proteins. Human MAGI cells (73), which are U373 (glioblastoma) cells stably expressing the HIV-1 receptors and thus permissive for HIV-1 infection, were retrovirally transduced to express huTRIM5 $\alpha$  or rhTRIM5 $\alpha$ . rhTRIM5 $\alpha$  was expressed at higher levels compared to huTRIM5 $\alpha$  (Fig. 6B), which may reflect intrinsic differences in expression levels of the two proteins, since similar observations were made in other cellular contexts (22, 46). HIV-1 was restricted  $\sim$ 41-fold in the cells transduced with rhTRIM5 $\alpha$  compared to control (“empty” vector-transduced) cells while, as expected, it was not restricted in cells transduced with huTRIM5 $\alpha$  (data not shown). Cells transduced with either of the two TRIM5 $\alpha$  orthologs or transduced with the empty vector were then infected with HIV-1<sub>NL43-IRES-GFP</sub> using amounts of the virus leading to ca. 0.1% infected cells and in the presence or absence of drug treatment. As shown Fig. 6A, nodocazole and paclitaxel increased the capacity of HIV-1 to infect cells transduced with rhTRIM5 $\alpha$  by  $(6.1 \pm 1.7)$ -fold and  $(12.1 \pm 4.5)$ -fold, respectively. The drugs had no significant effect on HIV-1 infectivity in the nonrestrictive control cells. Thus, integrity of the microtubule network is important for the efficient restriction by TRIM5 $\alpha$  regardless of the mechanism of virus entry.

**Loss of restriction is not caused by decreased TRIM5 $\alpha$  stability or by decreased cellular viability.** Next, we investigated a possible impact of the treatments on the turnover/stability of

TRIM5 $\alpha$ . HeLa cells stably expressing FLAG-rhTRIM5 $\alpha$  were either subjected to treatment with vehicle, nodocazole, paclitaxel, or EHNA or transfected with DHC or control siRNAs, using the same conditions as described above. *De novo* mRNA translation was inhibited using cycloheximide, and we monitored the decrease in protein levels for TRIM5 $\alpha$  and for actin as a control (Fig. 7A and B). We found that the turnover of TRIM5 $\alpha$  was not affected by the various treatments used. EHNA slightly decreased TRIM5 $\alpha$  levels at a single time point (1 h of cycloheximide treatment), while DHC depletion also slightly decreased TRIM5 $\alpha$  levels at 3 and 4.5 h of cycloheximide treatment (Fig. 7A). However, the results derived from three experiments revealed that these effects were not statistically significant (Fig. 7B).

Nodocazole, paclitaxel, and EHNA disrupt essential cellular functions, and it was thus important to ensure that the loss of restriction observed in our experimental conditions was not an artifact caused by gross cytotoxic effects. In all our infectivity assays, drugs are added for only 16 h and then removed, since only the first hours of infection are relevant to mechanisms of TRIM5 $\alpha$ -mediated restriction. Thus, we examined cellular viability after 16-h treatments of HeLa and FRhK-4 cells with increasing concentrations of nodocazole, paclitaxel, and EHNA (Fig. 7C). Viability was monitored using the XTT assay, a colorimetric method to measure cellular metabolic activity, in particular the activity of dehydrogenase enzymes (74). Both nodocazole and paclitaxel caused a progressive but relatively modest loss in viability, obviously reflecting a concentration-dependent inhibition of cell division (75, 76). At the relatively low concentrations used for infectivity assays, nodocazole caused an  $\sim$ 19% decrease in the viability of HeLa cells and an  $\sim$ 32% decrease in the viability of FRhK-4 cells (Fig. 7C). Similarly, paclitaxel caused an  $\sim$ 23% decrease in the viability of HeLa cells and an  $\sim$ 20% decrease in the viability of FRhK-4 cells at the concentrations used in our restriction assays (Fig. 7C). In both cases, the concentrations used were well below the threshold at which the decrease in viability becomes sharper, probably reflecting the occurrence of cytotoxic mechanisms in addition to the inhibition of cell division. Based on our XTT data, we would estimate these cytopathic effects to take place at concentrations greater than  $\sim$ 30  $\mu$ M for nodocazole and  $\sim$ 20  $\mu$ M for paclitaxel. We obtained a different pattern for EHNA: in both HeLa and FRhK-4 cells, viability decreased slowly to reach 85 to 90% of the control levels at a 1 mM concentration of the drug, but the drop in viability was much sharper at higher concentrations, and viability was fully lost at  $\sim$ 5 mM (Fig. 7C). At the concentrations used in our infectivity assays (600  $\mu$ M in HeLa cells, 1.2 mM in FRhK-4 cells), EHNA caused an  $\sim$ 12% decrease in viability in HeLa cells and an 8% decrease in FRhK-4 cells (Fig. 7C). Thus, even though these concentrations are close to the concentrations at which viability starts declining sharply, cellular viability is still at the level of untreated cells, and it is unlikely that the effects of EHNA on restriction result from its cytotoxicity.

**DHC depletion, nodocazole treatment, and paclitaxel treatment stabilize postentry HIV-1 cores.** A characteristic effect of TRIM5 $\alpha$ -mediated postentry retroviral restriction is the increase in the CA core disassembly of restriction-sensitive retroviruses, i.e., a decrease in core stability. We used the well-established fate-of-capsid assay (17, 22, 77) to analyze the impact of nodocazole treatment, paclitaxel treatment, and DHC depletion on TRIM5 $\alpha$ -mediated core disassembly. HeLa cells expressing rhTRIM5 $\alpha$  or mock transduced with the empty vector were exposed to HIV-

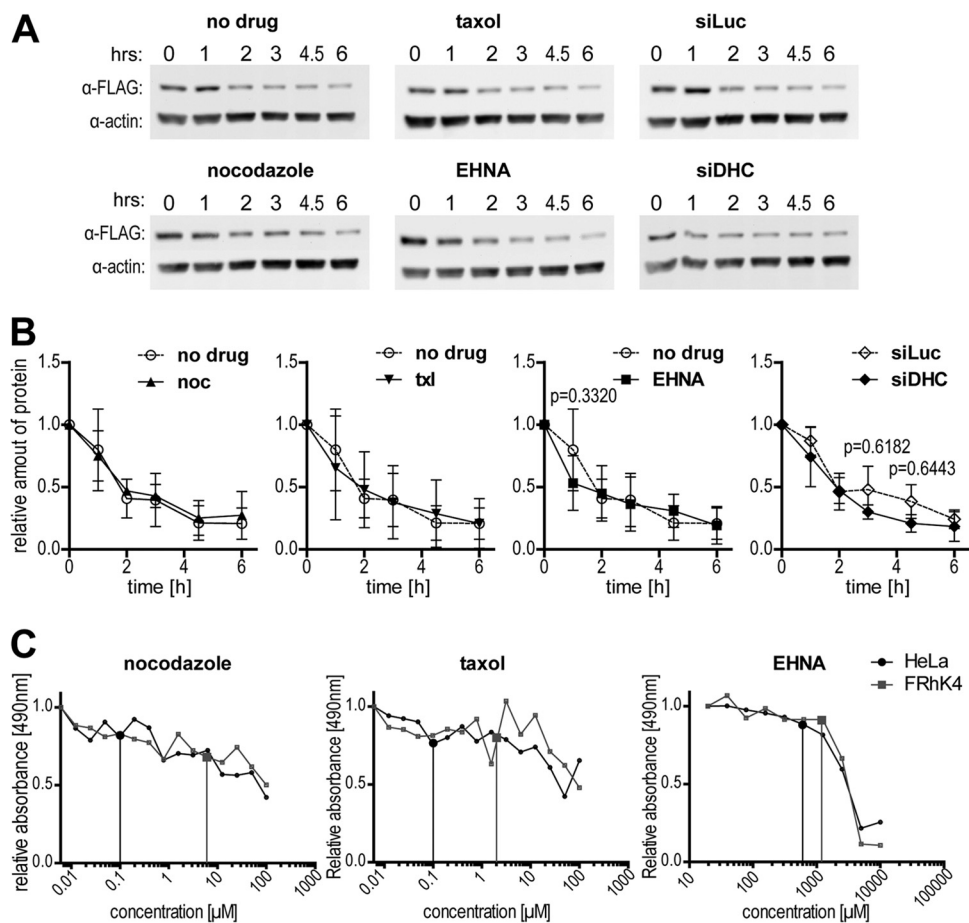


**FIG 7** Effect of treatments on TRIM5α stability and cell viability. (A) Effect on rhTRIM5α protein levels. HeLa cells stably expressing FLAG-tagged rhTRIM5α were treated with nocodazole (0.1 μM), paclitaxel (labeled “taxol” in panel A; 0.1 μM), EHNA (600 μM) and concomitantly treated with cycloheximide. Alternatively, cells were transfected with luciferase- or DHC-targeting siRNAs like before and treated with cycloheximide 72 h later. The efficiency of DHC knockdown was similar to that in Fig. 4A (not shown). Protein lysates were prepared at the indicated time points following the beginning of drug treatments. Lysates were subjected to Western blotting to detect FLAG-rhTRIM5α and actin. The results of one representative experiment of three independent experiments are shown. (B) Analysis of FLAG-rhTRIM5α protein turnover. FLAG-rhTRIM5α bands detected by Western blotting were quantified by densitometry and normalized to actin levels and then to the value obtained at the “0” time point; ctl, control; noc, nocodazole; txl, paclitaxel. Average data from three independent experiments with standard deviations are shown. The *P* values indicated on the graphs were calculated by using a Student *t* test for the three conditions in which an effect could be observed: EHNA treatment (1 h) and DHC siRNA transfection (3 and 4.5 h). (C) Cell viability assay. HeLa and FRhK-4 cells were treated with multiple concentrations of the indicated drugs for 16 h and cell viability was then determined using the XTT assay and normalized using the value obtained in the absence of drug as a reference. Vertical lines indicate the drug concentrations used in the present study, for each combination of drug and cell line. taxol, paclitaxel.

<sup>1</sup><sub>NL43</sub>-GFP in the presence or the absence of nocodazole, paclitaxel, or DHC siRNA. The efficiency of DHC knockdown was the same as in Fig. 4A (not shown). Cells were lysed and core-associated (pelletable) CA was isolated by ultracentrifugation through a sucrose cushion. The relative amounts of core-associated, soluble (postcentrifugation supernatant-associated), and total (whole-cell lysate [WCL]) CAP24 were assessed by densitometry of Western blots from three independent experiments (Fig. 8). The amounts of pelletable CA recovered were estimated relative to the total CA or relative to the soluble CA. As a control, cells were infected with a vector devoid of envelope proteins and thus incompetent for entry. Both virus preparations were normalized using a reverse transcription assay to ensure equal virus input. In the absence of the VSV G envelope, no or little CA signal was detectable in the infected cells, confirming that the CA detected was not associated with unfused viral particles (Fig. 8). As ex-

pected and in the absence of treatment, the relative amounts of pelletable CA cores were reduced in cells expressing rhTRIM5α, compared to the control cells transduced with the empty vector (Fig. 8). Specifically, the pellet/WCL CA ratios were reduced by 85.9% ± 9.0%, 70.4% ± 14.0%, and 75.7% ± 23.0%, respectively, in the experimental results shown Fig. 8A, B, and C. Similarly, the pellet/supernatant CA ratio was reduced by 85.0% ± 12.7%, 72.2% ± 11.5%, and 88.4% ± 9.1% in cells expressing rhTRIM5α (Fig. 8A to C, right panels, respectively). We observed that all of the treatments used had a stabilizing effect on postentry CA cores, both in permissive (control) cells and in restrictive (TRIM5α-expressing) cells (Fig. 8A to C). However, the increase in stability mediated by DHC depletion and paclitaxel treatment was greater in rhTRIM5α-expressing cells than in control cells, a finding consistent with the ability of these treatments to rescue infection. Specifically, DHC depletion in-

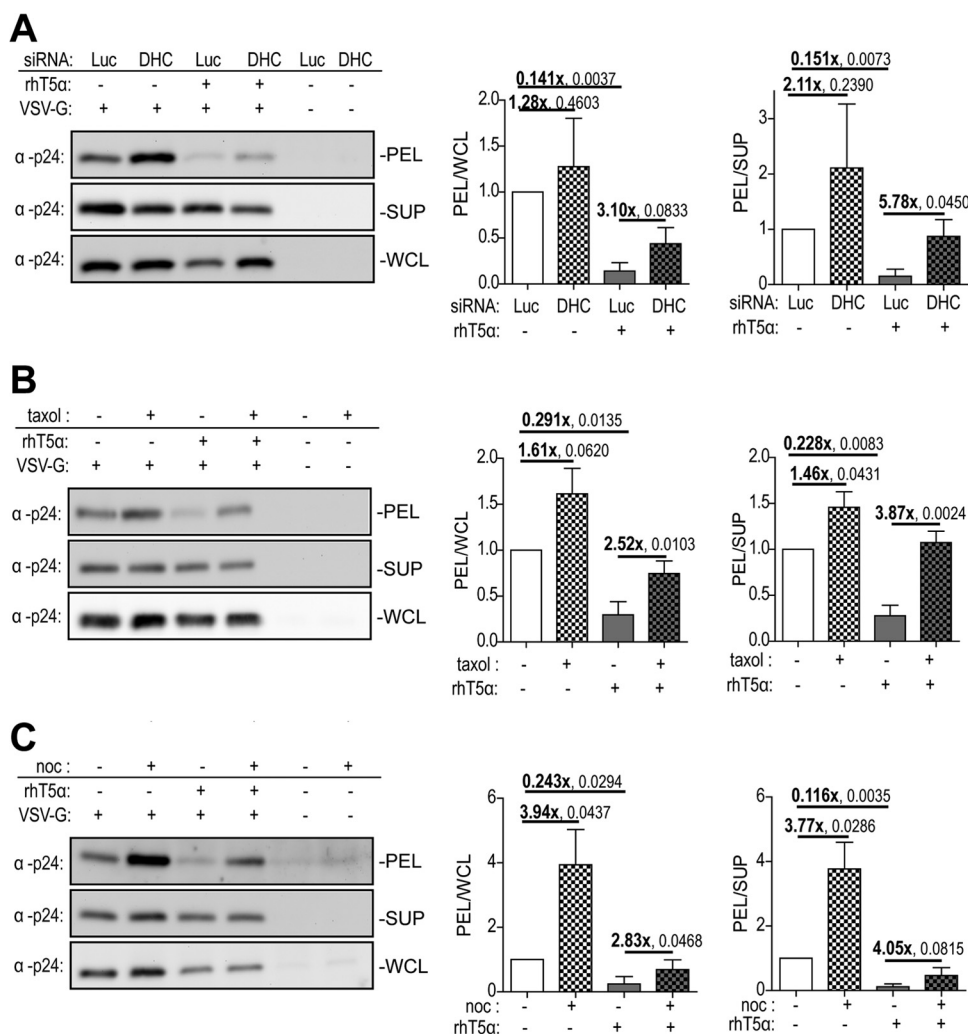


**FIG 8** DHC depletion, paclitaxel treatment, and nocodazole treatment increase the stability of HIV-1 cores in permissive or restrictive conditions. (A) HeLa cells stably expressing rhTRIM5 $\alpha$  (rhT5 $\alpha$ ) or transduced with the empty vector were transfected with the indicated siRNAs and 72 h later infected with HIV-1<sub>NL43-GFP</sub> or an entry-incompetent version of this vector lacking the VSV G envelope protein. Supernatants were replaced by fresh medium 2 h postinfection, and cells were lysed after an additional 4 h of incubation. Precleared lysates were layered on sucrose cushions, and particulate viral CA cores were pelleted by ultracentrifugation. Proteins in postcentrifugation pellets (PEL), supernatants (SUP), and whole-cell lysates (WCL) were analyzed by Western blotting to detect CA (p24). Bands corresponding to p24 were quantified by densitometry and plotted as pellet/WCL and pellet/supernatant ratios, relative to the nonrestrictive untreated control. Average data from three independent experiments with standard deviations are shown. The fold changes and *P* values (calculated using a Student *t* test) are shown for specific pairs of data. (B) Same as panel A, but the cells were treated or not with 0.1  $\mu$ M paclitaxel (taxol) during the 2 h of infection and during the 4 h of incubation. (C) Same as panel B, but cells were treated or not with 0.1  $\mu$ M nocodazole (noc).

creased the pellet/WCL CA ratio by 1.28-fold in control cells, whereas this increase was by 3.10-fold in rhTRIM5 $\alpha$ -expressing cells (Fig. 8A). Similarly, DHC depletion increased the pellet/supernatant CA ratio by 2.11-fold in control cells and by 5.78-fold in rhTRIM5 $\alpha$ -expressing cells (Fig. 8A). Paclitaxel treatment increased the pellet/WCL CA ratio by 1.61-fold in control cells, while the corresponding increase in rhTRIM5 $\alpha$ -expressing cells was 2.52-fold. Similarly, paclitaxel increased the pellet/supernatant CA ratio by 1.46-fold in control cells and by 3.87-fold in rhTRIM5 $\alpha$ -expressing cells (Fig. 8B). We obtained different effects for nocodazole, since treatment with this drug sharply increased CA core stability both in permissive and in restrictive conditions (Fig. 8C). Specifically, nocodazole increased the pellet/WCL CA ratio by 3.94-fold in control cells and by 2.83-fold in rhTRIM5 $\alpha$ -expressing cells. Similarly, the pellet/supernatant CA

ratio was increased by 3.77-fold in control cells and by about the same amount (4.05-fold) in rhTRIM5 $\alpha$ -expressing cells treated with this drug (Fig. 8C). Therefore, disrupting the microtubule network or the DHC motor has a stabilizing effect on postentry HIV-1 cores, which may decrease their susceptibility to TRIM5 $\alpha$ -mediated restriction. In addition, the magnitude of this stabilizing effect was greater in cells expressing rhTRIM5 $\alpha$  under treatment by paclitaxel or DHC siRNAs, which is consistent with these interventions specifically increasing HIV-1 infectivity in restrictive conditions. Nocodazole treatment increased postentry HIV-1 core stability equally in permissive and restrictive conditions, but its effect in permissive conditions was much stronger (3.94-fold) compared to DHC depletion (1.28-fold) or paclitaxel treatment (1.61-fold), perhaps masking the specific effect on restriction (see Discussion).

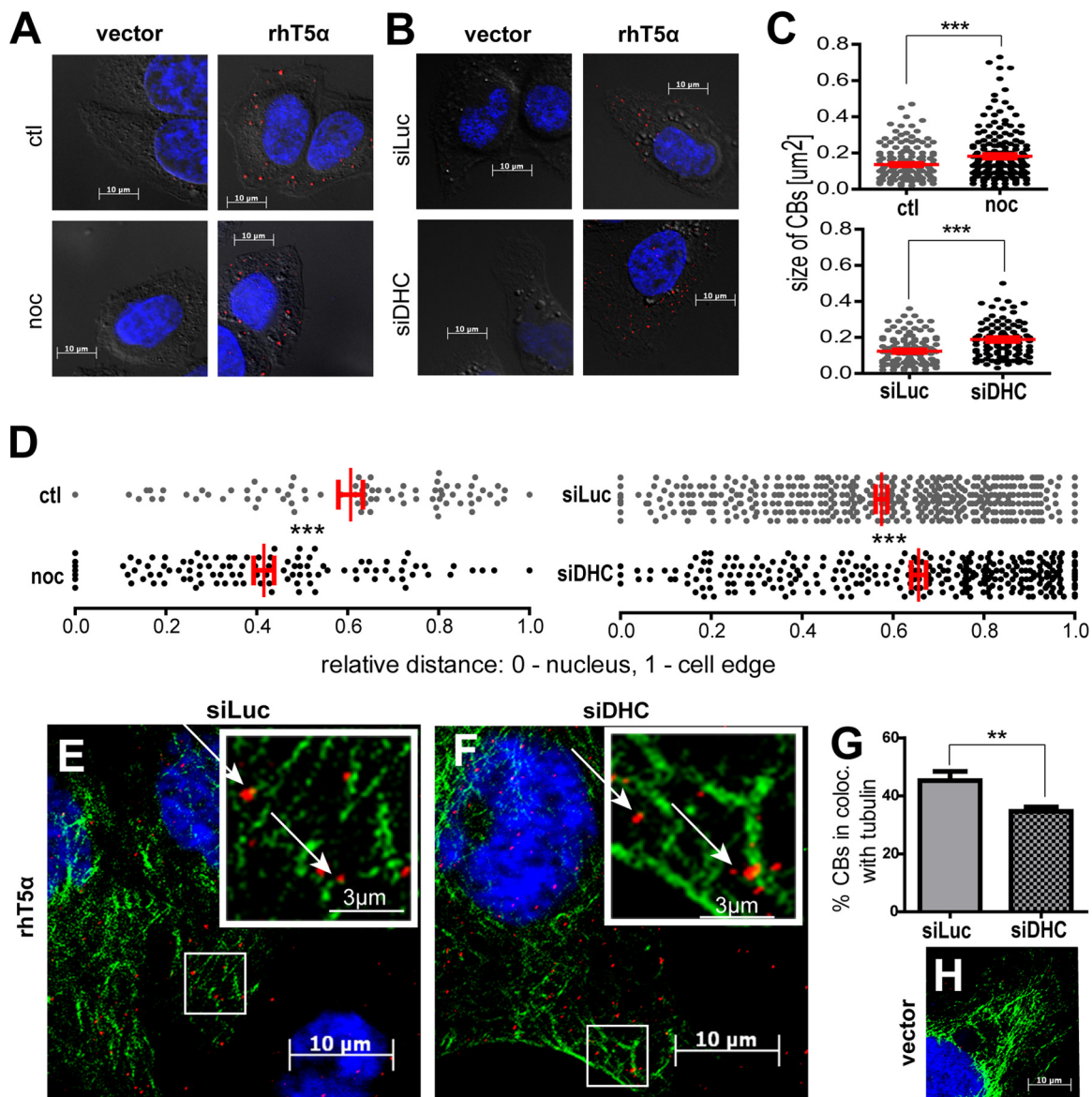


**FIG 9** Influence of DHC depletion and nocodazole treatment on the localization and dynamics of rhTRIM5α cytoplasmic bodies (CBs). (A and B) IF microscopy. HeLa cells transduced with FLAG-tagged rhT5α and control cells transduced with the empty vector were seeded on glass coverslips and 24 h later treated or not with 2 μM nocodazole for 6 h (A) or transfected with 40 nM siRNAs targeting DHC or Luc and 48 h later seeded on glass coverslips and incubated for an additional 24 h (B). Cells were fixed and immunostained for FLAG (red). DNA was stained with Hoechst 33342 (blue). Representative images are shown. (C) Sizes of CBs. All CBs were outlined in cells from a minimum of five randomly chosen fields, and their area was calculated using an image analysis software (AxioVision). Red bars show the standard errors of the mean (SEM). \*\*\*,  $P \leq 0.0001$  (Student *t* test). (D) The relative localization of all TRIM5α CBs from a minimum of five randomly chosen cells was calculated using the formula  $x/(x + y)$ , where  $x$  is the shortest distance to the nucleus, and  $y$  is the shortest distance to the cell's edge. SEM are shown as red bars. \*\*\*,  $P \leq 0.0001$ . (E to G) Colocalization of rhT5α CBs and microtubules. (E) HeLa cells transduced with FLAG-tagged rhTRIM5α were transfected with siRNAs targeting Luc or DHC, and 24 h later the cells were additionally transfected with a plasmid expressing GFP-α-tubulin. The next day, cells were seeded on glass coverslips and grown for 24 h. Cells were fixed and immunostained for FLAG (red) and DNA (blue). (F) Same as panel E, except that the cells were transduced with the empty vector and transfected with luciferase-targeting siRNA. Representative images are shown. Boxes in the top right corner show enlarged regions outlined on the images, and white arrows show examples of GFP-tubulin/FLAG-TRIM5α colocalizations. (G) Events of colocalization were quantified as a percentage of the total CBs in 10 randomly chosen fields. Bars represent the mean values from analyzed cells with SEM (\*\*,  $P < 0.005$ ).

**Effect of nocodazole treatment and DHC depletion on the size and localization of TRIM5 CBs.** The capacity of nocodazole treatment and DHC depletion to reduce TRIM5α-mediated restriction could stem from effects on the dynamics of TRIM5α, which would affect the size and/or localization of CBs. HeLa cells stably expressing FLAG-tagged rhTRIM5α were treated with no-

codazole or depleted for DHC and then stained for FLAG (Fig. 9A and B). The settings were adjusted to reveal CBs but not the diffuse FLAG signal. The size (area) of CBs (Fig. 9C) and their relative distances to the nucleus and to the “edge of cell” (Fig. 9D) were calculated as detailed in Materials and Methods. Nocodazole treatment and DHC knockdown increased the average size of

rhTRIM5 $\alpha$  CBs by  $33.9\% \pm 7.8\%$  and by  $52.6\% \pm 8.9\%$ , respectively (Fig. 9C). In addition, rhTRIM5 $\alpha$  CBs were found to be  $31.5\% \pm 3.7\%$  closer to the nucleus after nocodazole treatment (Fig. 9D). In contrast, DHC depletion caused a significant rhTRIM5 $\alpha$  CBs localization shift ( $14.2\% \pm 2.8\%$ ) toward the plasma membrane (Fig. 9D). The results presented in Fig. 9 show that the microtubule network is important for the dynamics of TRIM5 $\alpha$  CBs. Depletion of DHC and disruption of microtubules can have distinct effects on TRIM5 $\alpha$  CBs, but the increased peripheral localization of CBs seen upon DHC depletion suggests that dynein motor complexes are responsible for their retrograde transport. To test more directly whether dynein is involved in the association of TRIM5 $\alpha$  CBs with microtubules, we cotransfected HeLa cells stably expressing FLAG-rhTRIM5 $\alpha$  with siRNAs targeting either DHC or an irrelevant control and with a plasmid expressing GFP- $\alpha$ -tubulin and then stained for FLAG (Fig. 9E and F). Images were acquired with the Apotome system and deconvolved to facilitate analysis, and colocalization was quantified from multiple randomly chosen cells. The depletion of DHC resulted in a modest ( $23\% \pm 0.3\%$ ) and yet statistically significant decrease in the colocalization of rhTRIM5 $\alpha$  CBs and microtubules (Fig. 9G). Altogether, these results suggest that dynein motor complexes are involved in the association of TRIM5 $\alpha$  CBs with microtubules and in the retrograde transport of either TRIM5 $\alpha$  CBs.

## DISCUSSION

In this study, we examined the importance of microtubules and of the microtubule-associated dynein motor complexes in the restriction of HIV-1 and N-MLV by TRIM5 $\alpha$ . Pharmacological and siRNA-mediated depletion studies clearly show that the capacity of TRIM5 $\alpha$  to efficiently restrict incoming retroviruses is dependent on intact microtubules and a functioning dynein motor complex (Fig. 1 to 6). This was true regardless of (i) the retrovirus and TRIM5 $\alpha$  ortholog studied, (ii) whether TRIM5 $\alpha$  was expressed at endogenous levels or overexpressed through stable transduction, and (iii) the mechanism of virus entry. Nocodazole and paclitaxel, two drugs that disrupt the structure of the microtubule network through different mechanisms, had very similar, sometimes identical effects on retroviral restriction levels (Fig. 2 and 4). DHC depletion generally had a smaller effect on restriction than treatment with nocodazole or paclitaxel (Fig. 4), which may be due to the observed incomplete knockdown (Fig. 4A). However, DHC depletion did not synergistically inhibit TRIM5 $\alpha$  in the presence of either nocodazole (Fig. 4D) or paclitaxel (Fig. 4E), implying that these treatments all affected the same pathway. Finally, the observed impact of microtubules or dynein disruption on virus restriction was not caused by gross differences in expression levels or TRIM5 $\alpha$  stability (Fig. 7A and B) and was not a putative artifact stemming from cytotoxicity (Fig. 7C).

Destabilization of the viral CA core upon interaction with TRIM5 $\alpha$  is a hallmark of restriction and occurs in the hours following virus entry. We observed that DHC depletion, nocodazole treatment, and paclitaxel treatment all increased the relative amounts of pelletable CA, both in permissive and in restrictive conditions. This indicates that these treatments increase the stability of postentry HIV-1 CA cores. To our knowledge, this effect of interventions altering the cytoskeleton on HIV-1 disassembly had never been investigated before. Although the mechanism behind HIV-1 postentry CA core stabilization is unclear, it could

contribute to making HIV-1 partly resistant to TRIM5 $\alpha$  by counteracting the destabilizing effect of TRIM5 $\alpha$  (78). The increase in the relative amounts of core-associated CA induced by DHC depletion or paclitaxel treatment was greater in cells expressing rhTRIM5 $\alpha$  compared to control cells (Fig. 8A and B). This is consistent with these treatments specifically increasing HIV-1 infectivity in restrictive conditions. The results with nocodazole were more ambiguous, since this drug strongly increased the relative levels of core-associated CA (a 3- to 4-fold increase) both in permissive and in restrictive conditions (Fig. 8C). This apparent lack of specificity of nocodazole in this assay might be due to compounding effects of the drug. For instance, nocodazole could increase the apparent stability in permissive conditions through an additional mechanism that does not take place in restrictive conditions, hence masking the restriction-specific effect that is seen with DHC siRNAs or paclitaxel. Consistent with this, nocodazole increased the relative amounts of core-associated CA in permissive cells about twice as much as DHC depletion or paclitaxel treatment did.

Nocodazole treatment increased the size of TRIM5 $\alpha$  CBs and caused them to be positioned closer to the nucleus (Fig. 9), which is consistent with previous observations by Diaz-Griffero et al. (79). These data suggest that nocodazole interferes with the dynamics of TRIM5 $\alpha$  CBs, perhaps by preventing the exchange of TRIM5 $\alpha$  proteins between diffuse cytoplasmic population and CB-associated population (34). DHC depletion increased the average size of rhTRIM5 $\alpha$  CBs (Fig. 9C) but also caused CBs to accumulate toward the cell periphery (Fig. 9D). In addition, there was a modest but significant decrease in the association between microtubules and rhTRIM5 $\alpha$  (Fig. 9G). Altogether, these results suggest that the dynein motor translocates rhTRIM5 $\alpha$  CBs on microtubules and is at least partly responsible for their retrograde transport. When DHC is depleted, rhTRIM5 $\alpha$  CBs may shift toward the periphery of cells due to interactions with other molecular motors, such as the reverse polarity motor kinesin, which performs anterograde transport and can transport the same cargos as dynein does (80). Alternatively, DHC depletion could enhance the association of rhTRIM5 $\alpha$  with late endosomes, as was observed previously for components of the HIV-1 ribonucleoprotein such as Gag and the genomic RNA (57). Nocodazole treatment and DHC depletion showed distinct phenotypes with regard to TRIM5 $\alpha$ -mediated CA core disassembly (Fig. 8) and TRIM5 $\alpha$  CBs localization (Fig. 9D), and yet their effects on restriction are clearly not additive (Fig. 4). Thus, it is likely that these phenotypic differences simply reflect different mechanisms of action by which the two treatments inhibit a single pathway.

Perhaps surprisingly, the various interventions used in the present study generally had little effect on the transduction of HIV-1, SIVmac, and MLV vectors in permissive conditions. Nocodazole was originally reported to modestly inhibit the early stages of HIV-1 infectivity in MAGI cells (81). However, other studies demonstrated a lack of HIV-1 sensitivity to this drug in human embryo kidney 293T cells (82) and in CEM T cells (83). At first glance, such a lack of inhibition by nocodazole contradicts a role for microtubules in HIV-1 postentry intracellular transport (84). However, the existence of a population of nocodazole-resistant microtubules, which are less dynamic, has been described (85), raising the possibility that HIV-1 uses these specific microtubules for its transport. Likewise, depleting DHC had a small effect on the infection of human permissive HeLa cells by an SIV-

mac vector (Fig. 5B), and no effect was seen on the infection of HeLa cells by B-MLV (Fig. 4C) or HIV-1 (Fig. 5E) vectors. To the best of our knowledge, the only published evidence of a functional role for dynein motor complexes in HIV-1 postentry transport consisted in the injection of an antibody interfering with dynein motor function, leading to an ~50% decrease in HIV-1 movement toward the nucleus (84); however, this observation was not supported by infectivity data. Clearly, the precise mechanism of retroviral capsids transport toward the nucleus is yet to be determined (45). Regardless, our results show that disruption of the microtubule network and DHC depletion affect TRIM5 $\alpha$ -mediated restriction without strongly impairing infectivity in permissive cells, firmly establishing specificity. The effects seen on restriction probably stem from effects on TRIM5 $\alpha$  localization (Fig. 9), on CA stability (Fig. 8), or a combination of both.

## ACKNOWLEDGMENTS

We thank Maximilian Webers, Marie Leclerc, Maxime Veillette, Réjean Cantin, Pascal Jalaguer, Alexandre Deshière, and Mélodie B. Plourde for providing technical help. We thank Natacha Méridol, Mélodie B. Plourde, and Marie-Édith Nepveu-Traversy for critical readings of the manuscript. We acknowledge David N. Levy (University of Alabama at Birmingham) and Ali Saib (Université Paris, Paris, France) for sharing plasmid DNAs. The following reagents were obtained through the AIDS Research and Reference Reagent Program, Division of AIDS, National Institute of Allergy and Infectious Diseases, National Institutes of Health (NIH), Bethesda, MD: nevirapine (catalog no. 4666) and clone 183 p24 antibodies (catalog no. 3537, contributed by Bruce Chesebro).

M.J.T. holds a tier 1 Canada Research Chair in Human Immunodeficiency Retrovirology. This study was supported by grants from the Canadian Institutes of Health Research to A.J.M. (MOP-56974), M.J.T. (MOP-110960), and L.B. (MOP-102712).

## REFERENCES

- Hauler F, Mallery DL, McEwan WA, Bidgood SR, James LC. 2012. AAA ATPase p97/VCP is essential for TRIM21-mediated virus neutralization. *Proc. Natl. Acad. Sci. U. S. A.* 109:19733–19738. <http://dx.doi.org/10.1073/pnas.1210659109>.
- Kajaste-Rudnitski A, Marelli SS, Pultrone C, Pertel T, Uchil PD, Mechti N, Mothes W, Poli G, Luban J, Vicenzi E. 2011. TRIM22 inhibits HIV-1 transcription independently of its E3 ubiquitin ligase activity, Tat, and NF- $\kappa$ B-responsive long terminal repeat elements. *J. Virol.* 85:5183–5196. <http://dx.doi.org/10.1128/JVI.02302-10>.
- Uchil PD, Quinlan BD, Chan WT, Luna JM, Mothes W. 2008. TRIM E3 ligases interfere with early and late stages of the retroviral life cycle. *PLoS Pathog.* 4:e16. <http://dx.doi.org/10.1371/journal.ppat.0040016>.
- Wolf D, Goff SP. 2007. TRIM28 mediates primer binding site-targeted silencing of murine leukemia virus in embryonic cells. *Cell* 131:46–57. <http://dx.doi.org/10.1016/j.cell.2007.07.026>.
- Stremlau M, Owens CM, Perron MJ, Kiessling M, Autissier P, Sodroski J. 2004. The cytoplasmic body component TRIM5 $\alpha$  restricts HIV-1 infection in Old World monkeys. *Nature* 427:848–853. <http://dx.doi.org/10.1038/nature02343>.
- Hatziaannou T, Perez-Caballero D, Yang A, Cowan S, Bieniasz PD. 2004. Retrovirus resistance factors Ref1 and Lv1 are species-specific variants of TRIM5 $\alpha$ . *Proc. Natl. Acad. Sci. U. S. A.* 101:10774–10779. <http://dx.doi.org/10.1073/pnas.0402361101>.
- Keckesova Z, Ylinen LM, Towers GJ. 2004. The human and African green monkey TRIM5 $\alpha$  genes encode Ref1 and Lv1 retroviral restriction factor activities. *Proc. Natl. Acad. Sci. U. S. A.* 101:10780–10785. <http://dx.doi.org/10.1073/pnas.0402474101>.
- Song B, Javanbakht H, Perron M, Park DH, Stremlau M, Sodroski J. 2005. Retrovirus restriction by TRIM5 $\alpha$  variants from Old World and New World primates. *J. Virol.* 79:3930–3937. <http://dx.doi.org/10.1128/JVI.79.7.3930-3937.2005>.
- Perron MJ, Stremlau M, Song B, Ulm W, Mulligan RC, Sodroski J. 2004. TRIM5 $\alpha$  mediates the postentry block to N-tropic murine leukemia viruses in human cells. *Proc. Natl. Acad. Sci. U. S. A.* 101:11827–11832. <http://dx.doi.org/10.1073/pnas.0403364101>.
- Rahm N, Yap M, Snoeck J, Zoete V, Munoz M, Radespiel U, Zimmermann E, Michielin O, Stoye JP, Ciuffi A, Telenti A. 2011. Unique spectrum of activity of prosimian TRIM5 $\alpha$  against exogenous and endogenous retroviruses. *J. Virol.* 85:4173–4183. <http://dx.doi.org/10.1128/JVI.00075-11>.
- Yap MW, Nisole S, Lynch C, Stoye JP. 2004. Trim5 $\alpha$  protein restricts both HIV-1 and murine leukemia virus. *Proc. Natl. Acad. Sci. U. S. A.* 101:10786–10791. <http://dx.doi.org/10.1073/pnas.0402876101>.
- Asaoka K, Ikeda K, Hishinuma T, Horie-Inoue K, Takeda S, Inoue S. 2005. A retrovirus restriction factor TRIM5 $\alpha$  is transcriptionally regulated by interferons. *Biochem. Biophys. Res. Commun.* 338:1950–1956. <http://dx.doi.org/10.1016/j.bbrc.2005.10.173>.
- Carthage L, Parise MC, Ringard M, Chelbi-Alix MK, Hazan U, Nisole S. 2008. Implication of TRIM $\alpha$  and TRIMCyp in interferon-induced anti-retroviral restriction activities. *Retrovirology* 5:59. <http://dx.doi.org/10.1186/1742-4690-5-59>.
- Pertel T, Hausmann S, Morger D, Zuger S, Guerra J, Lascano J, Reinhard C, Santoni FA, Uchil PD, Chatel L, Bisiaux A, Albert ML, Strambio-De-Castillia C, Mothes W, Pizzato M, Grutter MG, Luban J. 2011. TRIM5 is an innate immune sensor for the retrovirus capsid lattice. *Nature* 472:361–365. <http://dx.doi.org/10.1038/nature09976>.
- Tareen SU, Emerman M. 2011. Human Trim5 $\alpha$  has additional activities that are uncoupled from retroviral capsid recognition. *Virology* 409:113–120. <http://dx.doi.org/10.1016/j.virol.2010.09.018>.
- Sebastian S, Luban J. 2005. TRIM5 $\alpha$  selectively binds a restriction-sensitive retroviral capsid. *Retrovirology* 2:40. <http://dx.doi.org/10.1186/1742-4690-2-40>.
- Stremlau M, Perron M, Lee M, Li Y, Song B, Javanbakht H, Diaz-Griffero F, Anderson DJ, Sundquist WI, Sodroski J. 2006. Specific recognition and accelerated uncoating of retroviral capsids by the TRIM5 $\alpha$  restriction factor. *Proc. Natl. Acad. Sci. U. S. A.* 103:5514–5519. <http://dx.doi.org/10.1073/pnas.0509961103>.
- Ganser-Pornillos BK, Chandrasekaran V, Pornillos O, Sodroski JG, Sundquist WI, Yeager M. 2011. Hexagonal assembly of a restricting TRIM5 $\alpha$  protein. *Proc. Natl. Acad. Sci. U. S. A.* 108:534–539. <http://dx.doi.org/10.1073/pnas.1013426108>.
- Luban J. 2007. Cyclophilin A, TRIM5, and resistance to human immunodeficiency virus type 1 infection. *J. Virol.* 81:1054–1061. <http://dx.doi.org/10.1128/JVI.01519-06>.
- Nisole S, Stoye JP, Saib A. 2005. TRIM family proteins: retroviral restriction and antiviral defense. *Nat. Rev. Microbiol.* 3:799–808. <http://dx.doi.org/10.1038/nrmicro1248>.
- Towers GJ. 2007. The control of viral infection by tripartite motif proteins and cyclophilin A. *Retrovirology* 4:40. <http://dx.doi.org/10.1186/1742-4690-4-40>.
- Bérubé J, Bouchard A, Berthouex L. 2007. Both TRIM5 $\alpha$  and TRIMCyp have only weak antiviral activity in canine D17 cells. *Retrovirology* 4:68. <http://dx.doi.org/10.1186/1742-4690-4-68>.
- Perron MJ, Stremlau M, Lee M, Javanbakht H, Song B, Sodroski J. 2007. The human TRIM5 $\alpha$  restriction factor mediates accelerated uncoating of the N-tropic murine leukemia virus capsid. *J. Virol.* 81:2138–2148. <http://dx.doi.org/10.1128/JVI.02318-06>.
- Roa A, Hayashi F, Yang Y, Lienlaf M, Zhou J, Shi J, Watanabe S, Kigawa T, Yokoyama S, Aiken C, Diaz-Griffero F. 2012. RING domain mutations uncouple TRIM5 $\alpha$  restriction of HIV-1 from inhibition of reverse transcription and acceleration of uncoating. *J. Virol.* 86:1717–1727. <http://dx.doi.org/10.1128/JVI.05811-11>.
- Kutluay SB, Perez-Caballero D, Bieniasz PD. 2013. Fates of retroviral core components during unrestricted and TRIM5-restricted infection. *PLoS Pathog.* 9:e1003214. <http://dx.doi.org/10.1371/journal.ppat.1003214>.
- Rold CJ, Aiken C. 2008. Proteasomal degradation of TRIM5 $\alpha$  during retrovirus restriction. *PLoS Pathog.* 4:e1000074. <http://dx.doi.org/10.1371/journal.ppat.1000074>.
- Anderson JL, Campbell EM, Wu X, Vandegraaff N, Engelman A, Hope TJ. 2006. Proteasome inhibition reveals that a functional preintegration complex intermediate can be generated during restriction by diverse TRIM5 proteins. *J. Virol.* 80:9754–9760. <http://dx.doi.org/10.1128/JVI.01052-06>.
- Diaz-Griffero F, Kar A, Lee M, Stremlau M, Poeschla E, Sodroski J. 2007. Comparative requirements for the restriction of retrovirus infection

- by TRIM5 $\alpha$  and TRIMCyp. *Virology* 369:400–410. <http://dx.doi.org/10.1016/j.virol.2007.08.032>.
29. Wu X, Anderson JL, Campbell EM, Joseph AM, Hope TJ. 2006. Proteasome inhibitors uncouple rhesus TRIM5 $\alpha$  restriction of HIV-1 reverse transcription and infection. *Proc. Natl. Acad. Sci. U. S. A.* 103:7465–7470. <http://dx.doi.org/10.1073/pnas.0510483103>.
  30. Campbell EM, Perez O, Anderson JL, Hope TJ. 2008. Visualization of a proteasome-independent intermediate during restriction of HIV-1 by rhesus TRIM5 $\alpha$ . *J. Cell Biol.* 180:549–561. <http://dx.doi.org/10.1083/jcb.200706154>.
  31. Danielson CM, Cianci GC, Hope TJ. 2012. Recruitment and dynamics of proteasome association with rhTRIM5 $\alpha$  cytoplasmic complexes during HIV-1 infection. *Traffic* 13:1206–1217. <http://dx.doi.org/10.1111/j.1600-0854.2012.01381.x>.
  32. Kar AK, Diaz-Griffero F, Li Y, Li X, Sodroski J. 2008. Biochemical and biophysical characterization of a chimeric TRIM21-TRIM5 $\alpha$  protein. *J. Virol.* 82:11669–11681. <http://dx.doi.org/10.1128/JVI.01559-08>.
  33. Li X, Sodroski J. 2008. The TRIM5 $\alpha$  B-box 2 domain promotes cooperative binding to the retroviral capsid by mediating higher-order self-association. *J. Virol.* 82:11495–11502. <http://dx.doi.org/10.1128/JVI.01548-08>.
  34. Campbell EM, Dodding MP, Yap MW, Wu X, Gallois-Montbrun S, Malim MH, Stoye JP, Hope TJ. 2007. TRIM5 $\alpha$  cytoplasmic bodies are highly dynamic structures. *Mol. Biol. Cell* 18:2102–2111. <http://dx.doi.org/10.1091/mbc.E06-12-1075>.
  35. Perez-Caballero D, Hatzioannou T, Zhang F, Cowan S, Bieniasz PD. 2005. Restriction of human immunodeficiency virus type 1 by TRIM-CypA occurs with rapid kinetics and independently of cytoplasmic bodies, ubiquitin, and proteasome activity. *J. Virol.* 79:15567–15572. <http://dx.doi.org/10.1128/JVI.79.24.15567-15572.2005>.
  36. Song B, Diaz-Griffero F, Park DH, Rogers T, Stremlau M, Sodroski J. 2005. TRIM5 $\alpha$  association with cytoplasmic bodies is not required for antiretroviral activity. *Virology* 343:201–211. <http://dx.doi.org/10.1016/j.virol.2005.08.019>.
  37. Lukic Z, Hausmann S, Sebastian S, Rucci J, Sastri J, Robia SL, Luban J, Campbell EM. 2011. TRIM5 $\alpha$  associates with proteasomal subunits in cells while in complex with HIV-1 virions. *Retrovirology* 8:93. <http://dx.doi.org/10.1186/1742-4690-8-93>.
  38. O'Connor C, Pertel T, Gray S, Robia SL, Bakowska JC, Luban J, Campbell EM. 2010. p62/sequestosome-1 associates with and sustains the expression of retroviral restriction factor TRIM5 $\alpha$ . *J. Virol.* 84:5997–6006. <http://dx.doi.org/10.1128/JVI.02412-09>.
  39. Moscat J, Diaz-Meco MT, Wooten MW. 2007. Signal integration and diversification through the p62 scaffold protein. *Trends Biochem. Sci.* 32:95–100. <http://dx.doi.org/10.1016/j.tibs.2006.12.002>.
  40. Seibenhener ML, Geetha T, Wooten MW. 2007. Sequestosome 1/p62: more than just a scaffold. *FEBS Lett.* 581:175–179. <http://dx.doi.org/10.1016/j.febslet.2006.12.027>.
  41. de Forges H, Bouissou A, Perez F. 2012. Interplay between microtubule dynamics and intracellular organization. *Int. J. Biochem. Cell Biol.* 44:266–274. <http://dx.doi.org/10.1016/j.biocel.2011.11.009>.
  42. Hook P, Vallee RB. 2006. The dynein family at a glance. *J. Cell Sci.* 119:4369–4371. <http://dx.doi.org/10.1242/jcs.03176>.
  43. Dodding MP, Way M. 2011. Coupling viruses to dynein and kinesin-1. *EMBO J.* 30:3527–3539. <http://dx.doi.org/10.1038/emboj.2011.283>.
  44. Hsieh MJ, White PJ, Pouton CW. 2010. Interaction of viruses with host cell molecular motors. *Curr. Opin. Biotechnol.* 21:633–639. <http://dx.doi.org/10.1016/j.copbio.2010.06.009>.
  45. Moulard AJ, Milev MP. 2012. Role of dynein in viral pathogenesis, p 561–583. *In* King SM (ed), *Dyneins: structure, biology, and disease*. Elsevier, New York, NY.
  46. Pham QT, Bouchard A, Grutter MG, Berthou L. 2010. Generation of human TRIM5 $\alpha$  mutants with high HIV-1 restriction activity. *Gene Ther.* 17:859–871. <http://dx.doi.org/10.1038/gt.2010.40>.
  47. Rusan NM, Fagerstrom CJ, Yvon AM, Wadsworth P. 2001. Cell cycle-dependent changes in microtubule dynamics in living cells expressing green fluorescent protein- $\alpha$ -tubulin. *Mol. Biol. Cell* 12:971–980. <http://dx.doi.org/10.1091/mbc.12.4.971>.
  48. Berthou L, Sebastian S, Sayah DM, Luban J. 2005. Disruption of human TRIM5 $\alpha$  antiviral activity by nonhuman primate orthologues. *J. Virol.* 79:7883–7888. <http://dx.doi.org/10.1128/JVI.79.12.7883-7888.2005>.
  49. Berthou L, Sebastian S, Sokolskaja E, Luban J. 2005. Cyclophilin A is required for TRIM5 $\alpha$ -mediated resistance to HIV-1 in Old World monkey cells. *Proc. Natl. Acad. Sci. U. S. A.* 102:14849–14853. <http://dx.doi.org/10.1073/pnas.0505659102>.
  50. Berthou L, Sebastian S, Sokolskaja E, Luban J. 2004. Lvl inhibition of human immunodeficiency virus type 1 is counteracted by factors that stimulate synthesis or nuclear translocation of viral cDNA. *J. Virol.* 78:11739–11750. <http://dx.doi.org/10.1128/JVI.78.21.11739-11750.2004>.
  51. Berthou L, Towers GJ, Gurer C, Salomoni P, Pandolfi PP, Luban J. 2003. As<sub>2</sub>O<sub>3</sub> enhances retroviral reverse transcription and counteracts Ref1 antiviral activity. *J. Virol.* 77:3167–3180. <http://dx.doi.org/10.1128/JVI.77.5.3167-3180.2003>.
  52. Naviaux RK, Costanzi E, Haas M, Verma IM. 1996. The pCL vector system: rapid production of helper-free, high-titer, recombinant retroviruses. *J. Virol.* 70:5701–5705.
  53. Sebastian S, Sokolskaja E, Luban J. 2006. Arsenic counteracts human immunodeficiency virus type 1 restriction by various TRIM5 orthologues in a cell type-dependent manner. *J. Virol.* 80:2051–2054. <http://dx.doi.org/10.1128/JVI.80.4.2051-2054.2006>.
  54. Zufferey R, Nagy D, Mandel RJ, Naldini L, Trono D. 1997. Multiply attenuated lentiviral vector achieves efficient gene delivery in vivo. *Nat. Biotechnol.* 15:871–875. <http://dx.doi.org/10.1038/nbt0997-871>.
  55. Imbeault M, Lodge R, Ouellet M, Tremblay MJ. 2009. Efficient magnetic bead-based separation of HIV-1-infected cells using an improved reporter virus system reveals that p53 upregulation occurs exclusively in the virus-expressing cell population. *Virology* 393:160–167. <http://dx.doi.org/10.1016/j.virol.2009.07.009>.
  56. Adachi A, Gendelman HE, Koenig S, Folks T, Willey R, Rabson A, Martin MA. 1986. Production of acquired immunodeficiency syndrome-associated retrovirus in human and nonhuman cells transfected with an infectious molecular clone. *J. Virol.* 59:284–291.
  57. Lehmann M, Milev MP, Abrahamyan L, Yao XJ, Pante N, Moulard AJ. 2009. Intracellular transport of human immunodeficiency virus type 1 genomic RNA and viral production are dependent on dynein motor function and late endosome positioning. *J. Biol. Chem.* 284:14572–14585. <http://dx.doi.org/10.1074/jbc.M808531200>.
  58. Luduena RF, Roach MC. 1991. Tubulin sulfhydryl groups as probes and targets for antimetabolic and antimicrotubule agents. *Pharmacol. Ther.* 49:133–152.
  59. Jordan MA, Wilson L. 2004. Microtubules as a target for anticancer drugs. *Nat. Rev. Cancer* 4:253–265. <http://dx.doi.org/10.1038/nrc1317>.
  60. Groschel B, Bushman F. 2005. Cell cycle arrest in G<sub>2</sub>/M promotes early steps of infection by human immunodeficiency virus. *J. Virol.* 79:5695–5704. <http://dx.doi.org/10.1128/JVI.79.5.5695-5704.2005>.
  61. Besnier C, Takeuchi Y, Towers G. 2002. Restriction of lentivirus in monkeys. *Proc. Natl. Acad. Sci. U. S. A.* 99:11920–11925. <http://dx.doi.org/10.1073/pnas.172384599>.
  62. Lin TY, Emerman M. 2008. Determinants of cyclophilin A-dependent TRIM5 $\alpha$  restriction against HIV-1. *Virology* 379:335–341. <http://dx.doi.org/10.1016/j.virol.2008.06.037>.
  63. Yoo S, Myszkowski DG, Yeh C, McMurray M, Hill CP, Sundquist WI. 1997. Molecular recognition in the HIV-1 capsid/cyclophilin A complex. *J. Mol. Biol.* 269:780–795. <http://dx.doi.org/10.1006/jmbi.1997.1051>.
  64. Stremlau M, Song B, Javanbakht H, Perron M, Sodroski J. 2006. Cyclophilin A: an auxiliary but not necessary cofactor for TRIM5 $\alpha$  restriction of HIV-1. *Virology* 351:112–120. <http://dx.doi.org/10.1016/j.virol.2006.03.015>.
  65. Hornick JE, Bader JR, Tribble EK, Trimble K, Breunig JS, Halpin ES, Vaughan KT, Hinchcliffe EH. 2008. Live-cell analysis of mitotic spindle formation in taxol-treated cells. *Cell Motil. Cytoskel.* 65:595–613. <http://dx.doi.org/10.1002/cm.20283>.
  66. Penningroth SM, Cheung A, Bouchard P, Gagnon C, Bardin CW. 1982. Dynein ATPase is inhibited selectively in vitro by erythro-9-[3-(2-hydroxy-nonyl)]adenine. *Biochem. Biophys. Res. Commun.* 104:234–240. [http://dx.doi.org/10.1016/0006-291X\(82\)91964-7](http://dx.doi.org/10.1016/0006-291X(82)91964-7).
  67. Zhang W, Greene W, Gao SJ. 2012. Microtubule- and dynein-dependent nuclear trafficking of rhesus rhadinovirus in rhesus fibroblasts. *J. Virol.* 86:599–604. <http://dx.doi.org/10.1128/JVI.06129-11>.
  68. Fukuda M. 1991. Lysosomal membrane glycoproteins. Structure, biosynthesis, and intracellular trafficking. *J. Biol. Chem.* 266:21327–21330.
  69. Burkhardt JK, Echeverri CJ, Nilsson T, Vallee RB. 1997. Overexpression of the dynamin (p50) subunit of the dynactin complex disrupts dynein-dependent maintenance of membrane organelle distribution. *J. Cell Biol.* 139:469–484. <http://dx.doi.org/10.1083/jcb.139.2.469>.
  70. He Y, Francis F, Myers KA, Yu W, Black MM, Baas PW. 2005. Role of

- cytoplasmic dynein in the axonal transport of microtubules and neurofilaments. *J. Cell Biol.* 168:697–703. <http://dx.doi.org/10.1083/jcb.200407191>.
71. Naldini L, Blomer U, Gage FH, Trono D, Verma IM. 1996. Efficient transfer, integration, and sustained long-term expression of the transgene in adult rat brains injected with a lentiviral vector. *Proc. Natl. Acad. Sci. U. S. A.* 93:11382–11388. <http://dx.doi.org/10.1073/pnas.93.21.11382>.
  72. He J, Chen Y, Farzan M, Choe H, Ohagen A, Gartner S, Busciglio J, Yang X, Hofmann W, Newman W, Mackay CR, Sodroski J, Gabuzda D. 1997. CCR3 and CCR5 are coreceptors for HIV-1 infection of microglia. *Nature* 385:645–649. <http://dx.doi.org/10.1038/385645a0>.
  73. Vodicka MA, Goh WC, Wu LI, Rogel ME, Bartz SR, Schweickart VL, Raport CJ, Emerman M. 1997. Indicator cell lines for detection of primary strains of human and simian immunodeficiency viruses. *Virology* 233:193–198. <http://dx.doi.org/10.1006/viro.1997.8606>.
  74. Scudiero DA, Shoemaker RH, Paull KD, Monks A, Tierney S, Nofziger TH, Currens MJ, Seniff D, Boyd MR. 1988. Evaluation of a soluble tetrazolium/formazan assay for cell growth and drug sensitivity in culture using human and other tumor cell lines. *Cancer Res.* 48:4827–4833.
  75. Jordan MA, Thrower D, Wilson L. 1992. Effects of vinblastine, podophyllotoxin, and nocodazole on mitotic spindles: implications for the role of microtubule dynamics in mitosis. *J. Cell Sci.* 102(Pt 3):401–416.
  76. Sorger PK, Dobles M, Tournebise R, Hyman AA. 1997. Coupling cell division and cell death to microtubule dynamics. *Curr. Opin. Cell Biol.* 9:807–814. [http://dx.doi.org/10.1016/S0955-0674\(97\)80081-6](http://dx.doi.org/10.1016/S0955-0674(97)80081-6).
  77. Ohkura S, Goldstone DC, Yap MW, Holden-Dye K, Taylor IA, Stoye JP. 2011. Novel escape mutants suggest an extensive TRIM5 $\alpha$  binding site spanning the entire outer surface of the murine leukemia virus capsid protein. *PLoS Pathog.* 7:e1002011. <http://dx.doi.org/10.1371/journal.ppat.1002011>.
  78. Black LR, Aiken C. 2010. TRIM5 $\alpha$  disrupts the structure of assembled HIV-1 capsid complexes in vitro. *J. Virol.* 84:6564–6569. <http://dx.doi.org/10.1128/JVI.00210-10>.
  79. Diaz-Griffero F, Li X, Javanbakht H, Song B, Welikala S, Stremlau M, Sodroski J. 2006. Rapid turnover and polyubiquitylation of the retroviral restriction factor TRIM5. *Virology* 349:300–315. <http://dx.doi.org/10.1016/j.virol.2005.12.040>.
  80. Muller MJ, Klumpp S, Lipowsky R. 2008. Tug-of-war as a cooperative mechanism for bidirectional cargo transport by molecular motors. *Proc. Natl. Acad. Sci. U. S. A.* 105:4609–4614. <http://dx.doi.org/10.1073/pnas.0706825105>.
  81. Bukrinskaya A, Brichacek B, Mann A, Stevenson M. 1998. Establishment of a functional human immunodeficiency virus type 1 (HIV-1) reverse transcription complex involves the cytoskeleton. *J. Exp. Med.* 188: 2113–2125. <http://dx.doi.org/10.1084/jem.188.11.2113>.
  82. Daniel R, Marusich E, Argyris E, Zhao RY, Skalka AM, Pomerantz RJ. 2005. Caffeine inhibits human immunodeficiency virus type 1 transduction of nondividing cells. *J. Virol.* 79:2058–2065. <http://dx.doi.org/10.1128/JVI.79.4.2058-2065.2005>.
  83. Yoder A, Guo J, Yu D, Cui Z, Zhang XE, Wu Y. 2011. Effects of microtubule modulators on HIV-1 infection of transformed and resting CD4 T cells. *J. Virol.* 85:3020–3024. <http://dx.doi.org/10.1128/JVI.02462-10>.
  84. McDonald D, Vodicka MA, Lucero G, Svitkina TM, Borisy GG, Emerman M, Hope TJ. 2002. Visualization of the intracellular behavior of HIV in living cells. *J. Cell Biol.* 159:441–452. <http://dx.doi.org/10.1083/jcb.200203150>.
  85. Schulze E, Kirschner M. 1987. Dynamic and stable populations of microtubules in cells. *J. Cell Biol.* 104:277–288. <http://dx.doi.org/10.1083/jcb.104.2.277>.